Stem Cell Reports
Article

OPEN ACCESS

Identification and Characterization of the Dermal Panniculus Carnosus Muscle Stem Cells

Neia Naldaiz-Gastesi,[1,2,3] María Goicoechea,[2,3] Sonia Alonso-Martín,[4] Ana Aiastui,[2,3] Macarena López-Mayorga,[5] Paula García-Belda,[3,6] Jaione Lacalle,[1,2,7] Carlos San José,[8] Marcos J. Araúzo-Bravo,[9,10] Lidwine Trouilh,[11,12,13] Véronique Anton-Leberre,[11,12,13] Diego Herrero,[14] Ander Matheu,[10,15] Antonio Bernad,[14] José Manuel García-Verdugo,[3,6] Jaime J. Carvajal,[5] Frédéric Relaix,[4] Adolfo Lopez de Munain,[2,3,16,17] Patricia García-Parra,[1,2,3,*] and Ander Izeta[1,18,*]

[1]Tissue Engineering Laboratory, Bioengineering Area
[2]Neuroscience Area
Instituto Biodonostia, San Sebastián 20014, Spain
[3]CIBERNED, Instituto de Salud Carlos III, Madrid 28029, Spain
[4]INSERM U955-E10, Université Paris Est, Faculté de Médicine, IMRB U955-E10, Creteil 94000, France
[5]Molecular Embryology Team, Centro Andaluz de Biología del Desarrollo, Sevilla 41013, Spain
[6]Laboratorio de Neurobiología Comparada, Instituto Cavanilles, Universidad de Valencia, Valencia 46980, Spain
[7]Faculty of Medicine and Nursing, UPV-EHU, San Sebastián 20014, Spain
[8]Animal Facility and Experimental Surgery
[9]Computational Biology and Systems Biomedicine
Instituto Biodonostia, San Sebastián 20014, Spain
[10]IKERBASQUE, Basque Foundation for Science, Bilbao 48013, Spain
[11]INSA, UPS, INP, LISBP, Université de Toulouse, 31077 Toulouse, France
[12]INRA, UMR792, Ingénierie des Systèmes Biologiques et des Procédés, 31400 Toulouse, France
[13]CNRS, UMR5504, 31400 Toulouse, France
[14]Immunology and Oncology Department, Spanish National Center for Biotechnology (CNB-CSIC), Madrid 28049, Spain
[15]Cellular Oncology Group, Oncology Area, Instituto Biodonostia, San Sebastián 20014, Spain
[16]Faculty of Medicine and Nursing, Department of Neurosciences, UPV-EHU, San Sebastián 20014, Spain
[17]Department of Neurology, Hospital Universitario Donostia, San Sebastián 20014, Spain
[18]Department of Biomedical Engineering, School of Engineering, Tecnun-University of Navarra, San Sebastián 20009, Spain
*Correspondence: pgarcia@nanogune.eu (P.G.-P.), ander.izeta@biodonostia.org (A.I.)
http://dx.doi.org/10.1016/j.stemcr.2016.08.002

SUMMARY

The dermal *Panniculus carnosus* (PC) muscle is important for wound contraction in lower mammals and represents an interesting model of muscle regeneration due to its high cell turnover. The resident satellite cells (the bona fide muscle stem cells) remain poorly characterized. Here we analyzed PC satellite cells with regard to developmental origin and purported function. Lineage tracing shows that they originate in *Myf5*$^{+}$, *Pax3*/*Pax7*$^{+}$ cell populations. Skin and muscle wounding increased PC myofiber turnover, with the satellite cell progeny being involved in muscle regeneration but with no detectable contribution to the wound-bed myofibroblasts. Since hematopoietic stem cells fuse to PC myofibers in the absence of injury, we also studied the contribution of bone marrow-derived cells to the PC satellite cell compartment, demonstrating that cells of donor origin are capable of repopulating the PC muscle stem cell niche after irradiation and bone marrow transplantation but may not fully acquire the relevant myogenic commitment.

INTRODUCTION

The dermal *Panniculus carnosus* (PC) muscle sits below the dermal fat layer and on top of the subcutaneous adipose tissue and fascia (Wojciechowicz et al., 2013). It is a fast-twitch muscle of vestigial nature in humans (Novakov et al., 2008), but otherwise ubiquitous in mammals. The PC has generally smaller fibers than other muscles with increased size heterogeneity and higher than usual regenerative myofibers (Brazelton et al., 2003). Being mainly composed of type II fibers, the PC muscle is thought to provide rodent loose skin with twitching and thermoregulation capacities (Greenwood, 2010), as well as promoting contraction (Watts et al., 1958) and supporting revascularization (Hughes and Dann, 1941) of full-thickness excisional wounds. Besides a long-sought clarification of its functional role, a better understanding of PC in animal models and humans would be instrumental for plastic surgery and subcutaneous drug delivery studies alike (McDonald et al., 2010). However, this unique muscle remains ill characterized. From the stem cell biology viewpoint, specific data on non-limb muscle satellite cells (the bona fide muscle stem cells) are scarce (Randolph and Pavlath, 2015). PC satellite cell biology may be particularly interesting as a model system due to the accessibility, dispensability for survival, and increased regeneration rate of this muscle. In addition, the PC is distinctively positioned to understand the physiological role (if any) of hematopoietic stem cell (HSC) fusion to myofibers and their differentiation after transplantation (Ferrari et al., 1998), a little studied phenomenon that may be related to exposure of fused HSC-derived nuclei to *MyoD*-expressing

myofibers (Dellavalle et al., 2011). In the absence of injury, the rate of bone marrow-derived cell incorporation to PC is highly significant when compared with the physiologically irrelevant rates achieved by other muscle groups (Brazelton et al., 2003; Corbel et al., 2003; Sherwood et al., 2004b). The reasons underlying the increased incorporation of non-resident cells to PC remain unclear but may be related to increased cellular turnover in the PC.

The exact developmental origin of PC satellite cells has yet to be determined. Throughout development of the trunk and limb muscles, there is continuity between fetal muscle "founder" cells and adult satellite cells, as the latter appear to derive from the central dermomyotome of the somite (Gros et al., 2005; Kassar-Duchossoy et al., 2005; Relaix et al., 2005; Schienda et al., 2006). Specifically, at the embryonic day 10.5 (E10.5) central dermomyotome in mice, En1^{+} cells generate muscle together with interscapular brown fat bundles and dermis (Atit et al., 2006). These data were confirmed by follow-up of *Pax7*^{CE}-*βGal*$^{+}$ cells traced at E9.5 that labeled the PC (Lepper and Fan, 2011). However, the specific contribution of these early embryonic precursors to the adult PC satellite cell pool remains unknown. In this work, we have analyzed the PC muscle stem cells with regard to developmental origin and purported function, as well as the contribution of bone marrow-derived cells to the PC satellite cell pool after bone marrow transplantation.

RESULTS

Dorsal PC Satellite Cells Belong to the *Myf5*$^{+}$ Cell Lineage and Express *Pax3*/*Pax7* during Development

The PC muscle sits below dermal adipose tissue in the mouse and is composed of striated fibers, as shown by the expression of *Mrf4* (alkaline phosphatase [AP])$^{+}$ (Kassar-Duchossoy et al., 2004) and sarcomeric myosin heavy chain (MyHC) (Figures 1A and 1B). The dorsal PC is known to arise from dermomyotomal precursors, but no lineage tracing study has yet addressed the origin of the canonical satellite cells in this muscle. Since a majority of adult muscle satellite cells derive from *Myf5*$^{+}$ progenitors (Biressi et al., 2013; Gayraud-Morel et al., 2012; Kuang et al., 2007) and express *Pax3*/*Pax7* at later stages, the use of *Myf5*, *Pax3*, and *Pax7* cell lineage-tracing models may help to dissect the cellular contribution at successive developmental stages (Figure 1C). To determine the developmental origin of PC, we crossed Cre recombinase-expressing transgenic lines with *R26YFP* and *ROSAmTmG* reporter mouse strains and pursued in situ localization of reporter-expressing cells by performing immunofluorescence analyses in dorsal skin sections. As expected, PC fibers expressed the fluorescent reporters when cells were marked by the *Myf5*Cre^{Sor}, *Pax3*$^{Cre/+}$, and *Pax7*$^{CreERT2/+}$ lineage-tracing constructs (Figures 1D–1F). By transmission electron microscopy (TEM), we confirmed that PC satellite cells were located below the basal lamina and presented electron-dense nuclei with highly condensed chromatin patches and relatively small and undifferentiated cytoplasm (Figure 1G, asterisk). In situ, PC satellite cells of adult skin express MYF5 but no detectable PAX3, as determined by the expression of surrogate marker nLacZ (nuclear localized LacZ; Figures 1H and 1I). As canonical satellite cells, PC satellite cells are PAX7^{+} (Figure 1J, higher-magnification image shown in inset 1J′) and derive from the *Myf5*$^{+}$ lineage (Figure 1K). However, we were concerned with the reportedly widespread expression of *R26YFP* when crossed with the *Myf5*$^{tm3(cre)Sor}$ mouse model (Eppig et al., 2015 and data not shown). To clarify tracing of *Myf5*$^{+}$ cell lineage, we generated and crossed a Cre-expressing mouse (*B195AP-Cre*) that marked a more restricted subset of *Myf5*$^{+}$ cells (Figure S1; more data on this strain are presented below). The more restricted *Myf5* lineage-tracing strain confirmed detection of EYFP^{+} cells in a satellite cell position, located between the plasmalemma and the basement membrane of the PC myofibers (Figure 1L). In summary, the lineage-tracing studies shown here confirm that, similar to other trunk muscles, PC satellite cells originate in *Myf5*$^{+}$, *Pax3*/*Pax7*$^{+}$ cell populations.

Muscle Cell Turnover Increases in Response to Injury to the PC with No Detectable Contribution of PC Satellite-Derived Cells to the Wound Bed

PC muscle is thought to be particularly regenerative, as determined by fiber morphology and the higher incorporation of bone marrow-derived cells compared with other muscles by cell-fusion events (Brazelton et al., 2003). To help us understand the determinants of PC turnover in homeostasis and response to wounding, we crossed *Pax7*$^{CreERT2/+}$ mice with the *ROSAmtmG* reporter line to trace the *Pax7*-derived lineage by EGFP expression over the short term after tamoxifen (TMX) induction (Figure 2A). Full-thickness skin-punch wounds (that included the epidermis, dermis, dermal fat, and PC layers; Figure 2B) were performed and histological sections of the wounded area analyzed at days 5 and 10 post injury (Figures 2C and 2D). In the negative control (absence of TMX), no EGFP^{+} fiber was detected in the PC (Figures 2E and 2H). After TMX injection but in the absence of injury, *Pax7* lineage tracing was induced and significant expression of the reporter gene under the control of *Pax7* was found within fibers, most likely as a result of the incorporation of *Pax7*-derived (EGFP^{+}) cells to PC myofibers (Figures 2F, 2I, 2K, and 2L). In response to wounding, EGFP^{+} myofibers further increased (Figures 2G, 2J, and 2M) indicating that, while the PC seems to be markedly regenerative even under homeostatic

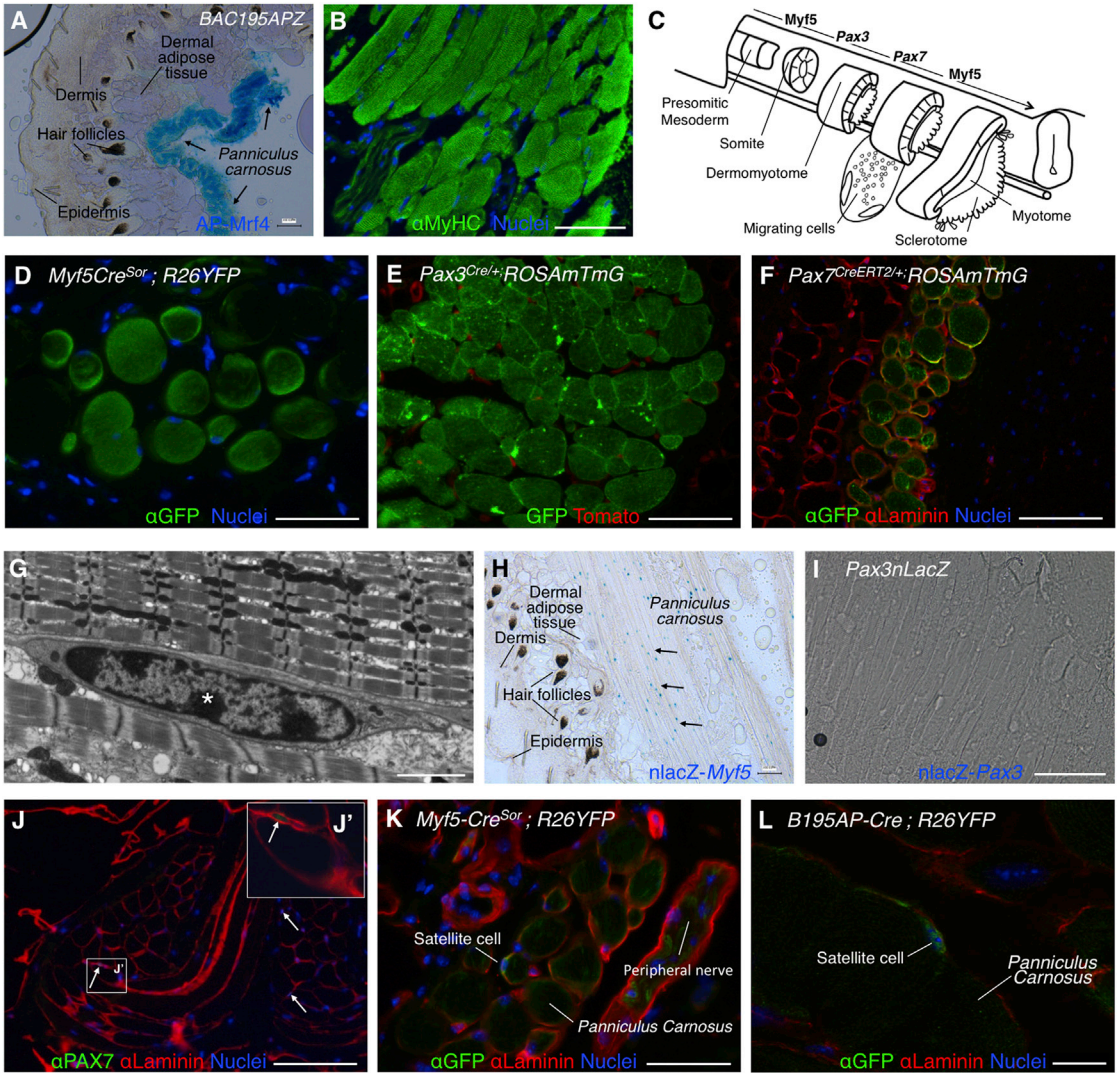

Figure 1. Elucidation of the Developmental Origin of PC Muscle and Satellite Cells

(A and B) Structure and localization of the PC. Histological sections of dorsal skin showing the presence of AP-*Mrf4*$^{+}$ fibers (in *B195APZ* mice) (A) and striated MyHC^{+} fibers (in wild-type mice) (B).

(C) Schematic representation of embryonic muscle development from presomitic mesoderm to myotome formation (modified from Buckingham and Rigby, 2014). Sequential expression of *Myf5* (at the PSM), *Pax3*, *Pax7*, and again *Myf5* (at the somite) transcription factors is depicted at the top.

(D) *Myf5*$^{+}$ lineage traced by immunofluorescence with anti-GFP antibody of *Myf5Cre*^{SOR}*;R26YFP* dorsal skin sections.

(E) *Pax3*$^{+}$ lineage traced by fluorescence of GFP and Tomato in *Pax3*$^{Cre/+}$ dorsal skin sections.

(F) *Pax7*$^{+}$ lineage traced by immunofluorescence with anti-GFP and anti-Laminin antibodies of *Pax7*^{CE} dorsal skin sections.

(G) TEM image of PC satellite cell ultrastructure from ultrathin skin sections. Asterisk indicates condensed chromatin patch.

(H) Histological section of dorsal skin showing the localization of nlacZ-*Myf5*$^{+}$ cells (arrows) (in *B195APZ* mice).

(I) In *Pax3nLacZ* mice, no staining of the PC was observed indicating that PC satellites are nlacZ-*Pax3*-negative cells.

(J) Immunofluorescence with anti-PAX7 antibody demonstrates *Pax7*$^{+}$ cells (arrows) in a satellite cell position underlying Laminin^{+} basement membrane. (J′) Higher-magnification inset.

(K) Satellite cell marked by anti-GFP antibody in *Myf5Cre*^{SOR}*;R26YFP* mice.

(L) Satellite cell marked by anti-GFP antibody in *B195AP-Cre;R26YFP* mice. Nuclei were counterstained with Hoechst 33258 (blue). Scale bars represent 100 μm in all panels with the exception of (G) (2 mm) and (L) (10 μm). See also Figure S1.

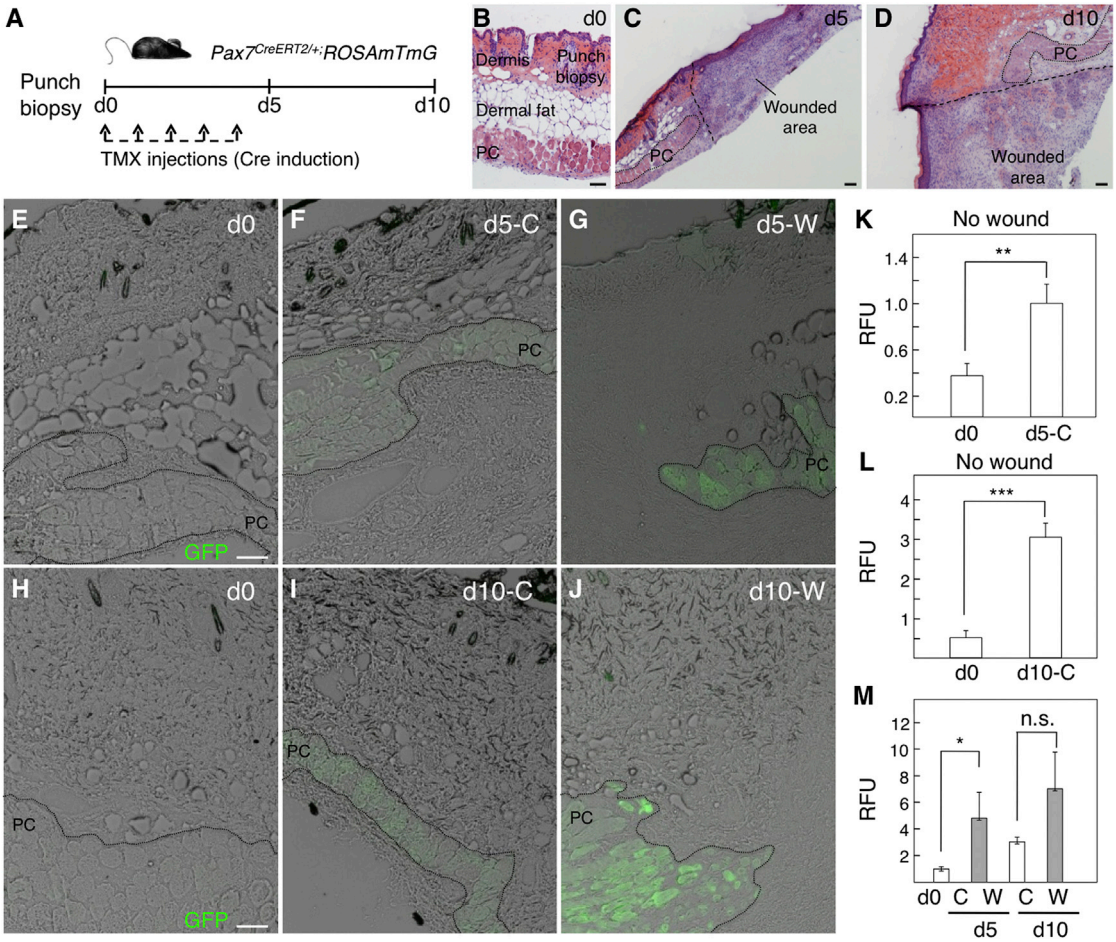

Figure 2. Characterization of the PC Regenerative Capacity in Homeostasis and in Short-Term Response to Wounding

(A) Outline of experimental design.

(B–D) Dorsal skin sections stained with H&E show the punch biopsy at day (d) 0 (B), and the wounded area at day 5 (C) and day 10 (D) post injury.

(E–J) GFP fluorescence in histological sections showing a control (C) area at day 0 (E and H), day 5 (F), and day 10 (I), and showing a wounded (W) area at day 5 (G) and day 10 (J).

(K–M) Quantification of the relative fluorescence units (RFU) present in the PC area. Comparisons between RFU of day 0 and day 5 in a control area (K), between day 0 and day 10 in a control area (L), and between control areas at days 0, 5, and 10 and wound areas at days 5 and 10 (M) are shown. Bars represent means ± SD in which the RFU were calculated in ImageJ from one to seven independent sections (N = 3 mice; n = 1 experiment). *$p < 0.05$, **$p < 0.01$, ***$p < 0.001$; n.s., not significant.

Scale bars, 100 μm.

conditions, the insult induced a further increase in cell turnover within the PC and the formation of new fibers.

A putative role of activated PC satellite cell progeny in wound contraction has been suggested (Munz et al., 1999), although to our knowledge direct contribution of PC-derived cells to the newly formed granulation tissue has not been experimentally observed. To test whether the PC satellite cell progeny contributes to the wound bed, we induced *Pax7*$^{CreERT2/+}$;*ROSAmTmG* mice with TMX 1 month in advance to ensure that all PC satellites were traced by *EGFP* expression (Figure 3A), and full-thickness punch biopsies were performed as before (Figures 3B–3D). In this long-term assay, no contribution of PC satellite cell-derived (EGFP$^+$) cell was evident in the wound bed up to day 10 post injury (Figures 3E–3L). Since regenerative fibers may be distinguished by the expression of embryonic forms of myosin (Schiaffino et al., 2015), staining with anti-MyHC3 antibody (DiMario et al., 1991) confirmed the existence of numerous regenerative myofibers in the PC (Figure S2). These results indicated that PC satellite cells are committed to muscle regeneration upon skin and muscle wounding, and that their progeny does not contribute

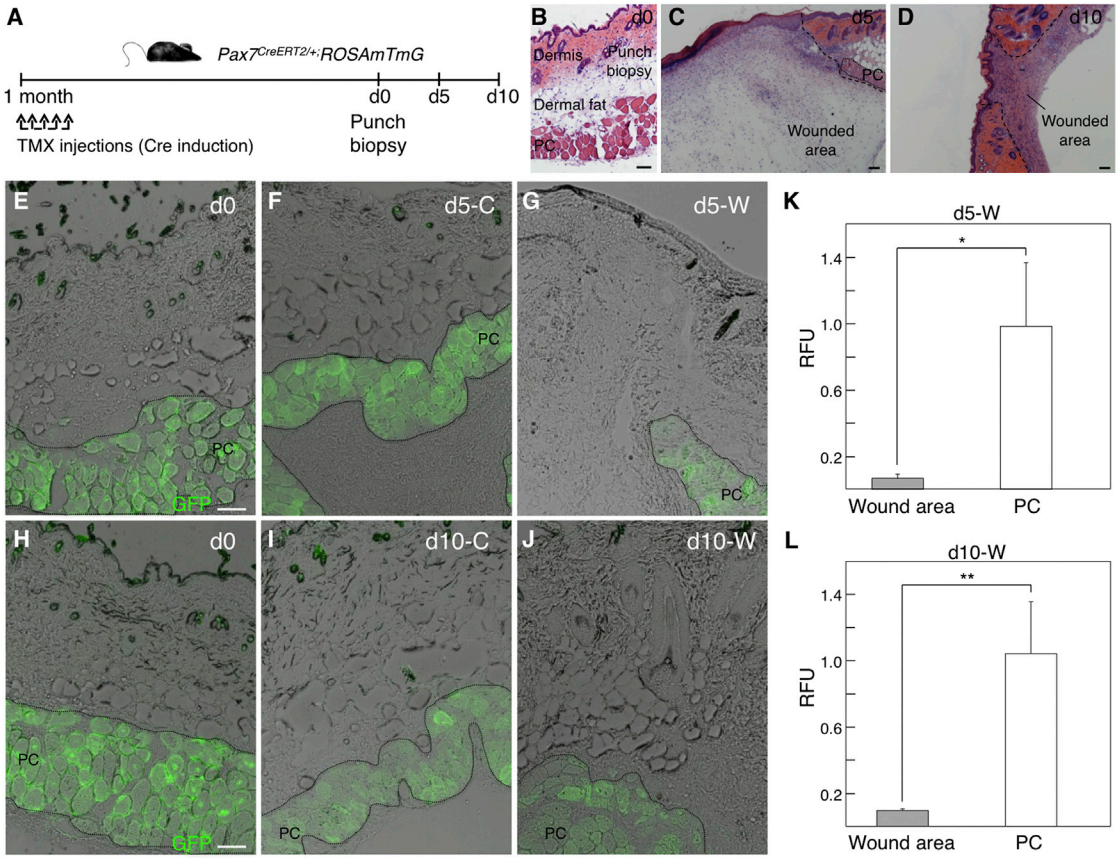

Figure 3. No Detectable In Vivo Contribution of PC-Derived Satellite Cells to the Dermal Compartment in Homeostasis or in Long-Term Response to Wounding

(A) Outline of experimental design. d, day; TMX, tamoxifen.

(B–D) Dorsal skin sections stained with H&E show the punch biopsy at day 0 (B), and the wounded area at day 5 (C) and day 10 (D) post injury.

(E–J) GFP fluorescence in histological sections showing a control (C) area at day 0 (E and H), day 5 (F), and day 10 (I), and showing a wounded (W) area at day 5 (G) and day 10 (J).

(K and L) Quantification of the relative fluorescence units (RFU) present in the PC and wound areas. Comparisons between RFU at PC and wound (W) areas at days 5 (K) and 10 (L) are shown. Bars represent means ± SD in which the RFU were calculated in ImageJ from two to seven independent sections (N = 3 mice; n = 1 experiment). *$p < 0.05$, **$p < 0.01$.

Scale bars, 100 μm. See also Figure S2.

to the wound bed and thus presents no obvious role in promoting full-thickness wound contraction.

Contribution of Bone Marrow-Derived Cells to the PC Satellite Cell Compartment

An intriguing possibility unresolved by previous studies was that bone marrow-derived cells, which engraft in significant numbers into PC muscle in the absence of injury (Brazelton et al., 2003), could contribute to the adult PC satellite cell pool. BMI1 is a transcription factor that is expressed in most adult stem cells, including satellite cells of skeletal muscle (Robson et al., 2011). To analyze whether bone marrow-derived cells contributed to the PC satellite cell pool, we used recipient *Bmi1-Cre;YFP* mice (i.e., animals expressing YFP in satellite cells) that had been irradiated and successfully transplanted with donor RFP^+ bone marrow cells from *Act-RFP* mice (Figure 4A; Valiente-Alandi et al., 2015). As expected, animals transplanted with bone marrow showed a sizable contribution of RFP^+ cells to the PC myofibers (6.95% positive fibers), which was within the expected range (Figures 4B and 4C; Brazelton et al., 2003). Importantly, the contribution of donor cells to the satellite cell compartment had not been previously analyzed. We detected cells of donor origin in a satellite position (RFP^+; Figure 4D) in the PC muscle of transplant recipients. To shed light on their functional

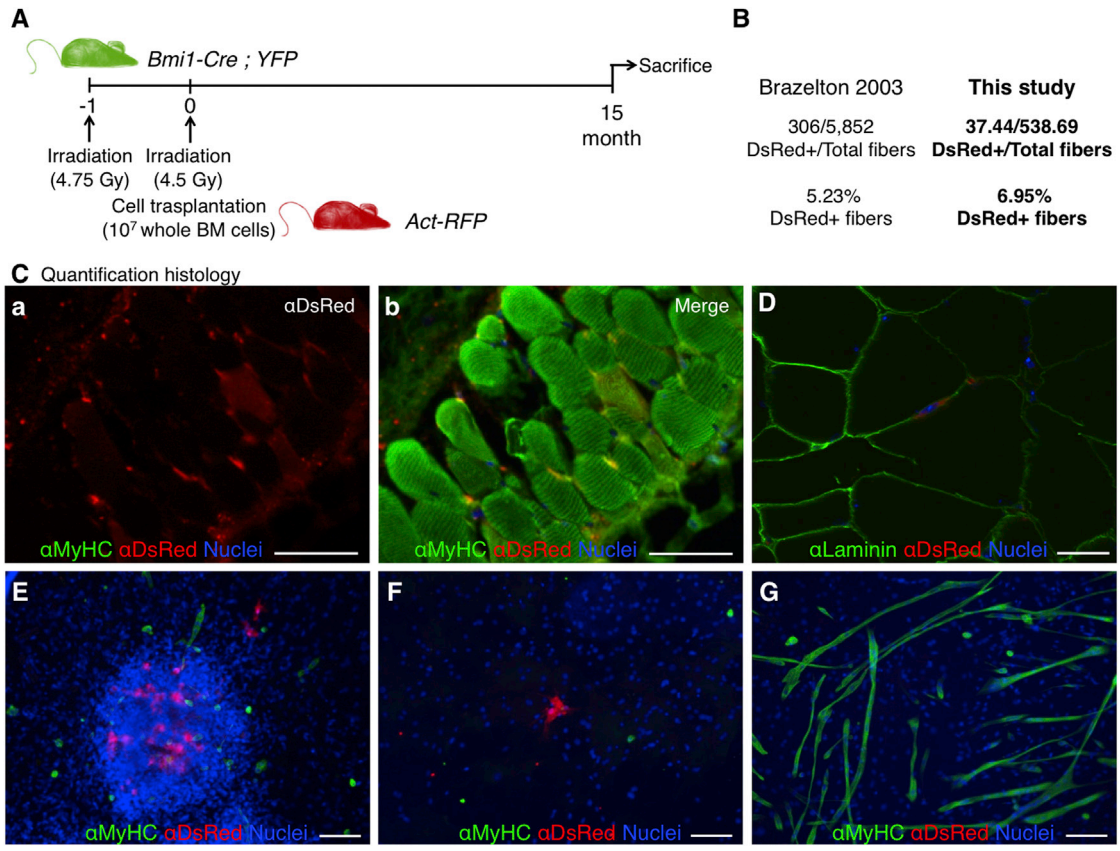

Figure 4. Contribution of Bone Marrow-Derived Cells to PC Fibers 15 Months after Bone Marrow Transplantation

(A) Outline of experimental design. Mice expressing YFP in *Bmi1*$^+$ cell lineage were transplanted with RFP$^+$ bone marrow (Valiente-Alandi et al., 2015).

(B) Quantification of DsRed-positive bone marrow-derived cell incorporation into PC in this study yielded results similar to those of Brazelton et al. (2003), i.e., higher than usual in vivo incorporation.

(C) Immunofluorescence detection of donor-derived RFP$^+$ fibers with anti-DsRed and sarcoplasmic anti-myosin heavy-chain (MyHC, all fibers) antibodies showing the red channel (a) and the merged channels (b).

(D) Histological sections of dorsal skin showing a DsRed$^+$ cell in a satellite cell position below Laminin$^+$ basement membrane.

(E–G) The lack of contribution of bone marrow-derived cells to striated muscle differentiation in vitro was demonstrated by immunofluorescence with anti-DsRed and sarcoplasmic anti-myosin heavy-chain (MyHC, all fibers) antibodies. Nuclei were counterstained with Hoechst 33258 (blue).

Scale bars, 100 μm.

status, we took advantage of the fact that robust striated muscle derivation (in vitro and in vivo) is obtained from dermis-derived sphere cultures (Garcia-Parra et al., 2014; Qiu et al., 2010; Wakabayashi et al., 2010). In fact, we previously hypothesized that those cultures expanded the PC satellite cells (Garcia-Parra et al., 2014). In vitro culture of dermal sphere cells from the RFP$^+$ bone marrow-transplanted mice in myogenic conditions demonstrated no contribution of donor bone marrow cell progeny to the formed myotubes (Figures 4E–4G). These results indicated that cells of donor origin are capable of repopulating the muscle stem cell niche but may not fully acquire the relevant myogenic commitment. However, a better understanding of the process of myotube derivation from dermis-derived cultures was needed to ascertain their apparent loss of functionality.

PC Satellite Cell Progeny Is Enriched in Dermal Precursor Sphere Cultures

Because the identity of the myogenic cell in dermal precursor sphere cultures remains uncertain, we examined dermal spheres at the ultrastructural level by TEM (Figures 5A–5C). At day 7 of proliferation culture, two distinct cell subpopulations were observed: a majority of cells presented vacuoles (Figure 5A, black asterisks) while a second, minor population (10%–15%) did not (Figure 5A, white asterisks).

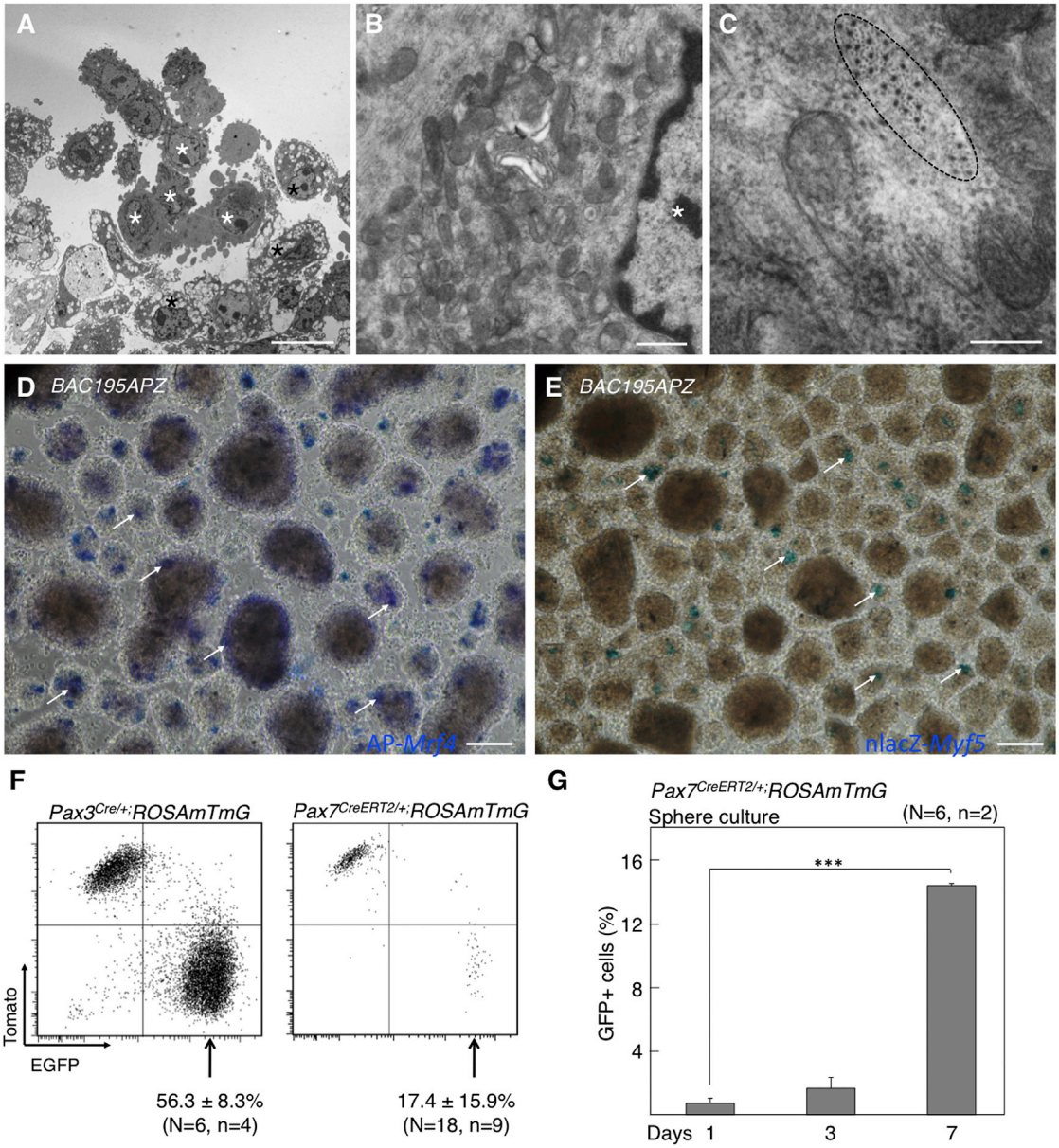

Figure 5. PC Satellite Cell Progeny Is Enriched in Dermal Precursor Sphere Cultures

(A–C) TEM images of dermal spheres. Cells with distinctive morphologies are marked by black and white asterisks. Actomyosin filaments are encircled in (C).

(D and E) Detection of AP-*Mrf4*$^{+}$ (D) and nlacZ-*Myf5*$^{+}$ (E) cells in dermal sphere cultures. Positive cells are marked by arrows.

(F) Flow cytometry analyses of mTomato- and mEGFP-expressing cells from *Pax3Cre* and *Pax7*^{CE} mice. Data represent mean ± SD. The experiments were independently replicated as specified (N, mice; n, experiments).

(G) Percentage of GFP^{+} cells by flow cytometry at 1, 3, and 7 days of dermosphere cultures. Bars represent means ± SD. ***$p < 0.001$. Scale bars represent 10 mm in (A), 500 nm in (B), 200 nm in (C), and 100 μm in (D) and (E). See also Figures S3 and S4.

Vacuole-rich cells had a phenotype consistent with immature fibroblasts (Figure 5B). In contrast, low-vacuole cells (white asterisks) were more rounded, had less heterochromatic nuclei, and presented abundant perinuclear mitochondria and undilated rough ER, consistent with a myogenic fate (Mauro, 1961; Nag and Foster, 1981). Accordingly, actomyosin filaments could only be seen in the latter cells (Figure 5C).

To understand their origin and in vitro expansion, we analyzed dermal myogenic precursors in *B195APZ* mice

that express nLacZ and cytoplasmic AP driven by the full *Myf5* and *Mrf4* regulatory regions, respectively (Carvajal et al., 2001). At day 7 of proliferative culture, AP^+ and $\beta\text{-Gal}^+$ cells were detected in dermal spheres (Figures 5D and 5E; arrows). Furthermore, lineage-tracing studies of $Pax3^+$ and $Pax7^+$ cells demonstrated their presence in dermal sphere cultures (Figure 5F; but see below with regard to $Pax3^+$ cells). To test for a possible enrichment of PC satellite-derived cells during sphere culture, we used the inducible *Pax7* mouse model and quantified $Pax7^+$ cells at different times of sphere proliferation (Figure 5G). There was at least 15-fold enrichment in the proportion of GFP $(Pax7)^+$ cells in the 7 days of sphere culture, indicating that dermal myogenic precursors have an advantage over other sphere cells in survival and/or proliferation rates. We also looked at the capacity for myotube derivation of PC-derived satellite cells compared with limb muscle (tibialis anterior [TA])-derived cells (Figure S3A). For this comparison, it must be taken into account that the vast amount of non-myogenic cells in dermis-derived cultures dilutes the number of PC satellite cells, which is about 15% at day 7 of proliferation culture (Figure 5G). In contrast, the number of satellite cells in myospheres is much greater (about 70% [Sarig et al., 2006]). Real-time qPCR analysis for mRNA expression of myogenic genes showed a significant (approximately 3-fold) upregulation of myogenic genes in differentiated cultures from TA compared with PC (Figure S3B), which indicates that PC-derived satellite cells have a myogenic capacity similar to that of TA-derived satellite cells. Finally, the contribution of PC satellite cells to myotubes was quantified in differentiation culture. The percentage of mono- and multinucleated cells derived from the $Pax7^+$ lineage was quantified at days 1, 3, and 7 of differentiation, demonstrating significant incorporation of GFP^+ cells into the developing myotubes (Figure S3C). In summary, a significant enrichment of PC satellite cell progeny that retained myogenic capacity was detected in dermis-derived sphere cultures.

PC Satellite Cell Progeny Is the Only Cell Population Responsible for Dermis-Derived Myogenesis In Vitro

Dermis-derived sphere cultures are highly heterogeneous (Etxaniz et al., 2014). To confirm the identity of the myogenic progenitor, we placed dermal spheres (unsorted cultures) into striated muscle differentiation conditions (Figure S4). After 7-day unsorted differentiation culture of *BAC195APZ* spheres, all myotubes were $Mrf4(AP)^+$ (Figure S4A). $Myf5(\beta\text{-Gal})^+$ cells appeared as mononucleated myoblasts or juxtaposed to differentiating myotubes (Figure S4B). Lineage tracing of the $Myf5Cre^{Sor}$, $Pax3^{Cre/+}$, *B195AP-Cre*, and $Pax7^{CreERT2/+}$ constructs showed in all cases a contribution of these cell lineages to dermis-derived myotubes (Figures S4C–S4F). Importantly, no $MyHC^+$ myotubes negative for any of the reporter genes were detected, indicating that they all derived from PC satellite cells.

To study whether perivascularly localized cells present in the dermis or PC muscle also contribute to striated muscle derivation, we traced the perivascular cells by chondroitin sulfate proteoglycan 4 (*Cspg4*, coding for NG2) expression (Figure S4G). This construct traced interstitial cells within the PC muscle (Figure S4Ga) that did not give $EYFP^+$ myotubes in unsorted cultures (Figure S4Gb) or after sorting of positive and negative EYFP fractions (Figures S4Gc and S4Gd). To analyze this in a more quantitative manner, mRNA was extracted from fluorescence-activated cell sorting (FACS)-sorted cell fractions and the relative expression of myogenic genes was quantified by qRT-PCR (Figure S4Ge). As expected, the myogenic marker mRNAs were preferentially upregulated in the $Cspg4^-$ cell fraction, indicating no contribution of perivascular cells to dermal myogenesis.

To confirm the contribution of PC satellite cells to dermal myogenesis, we sorted by FACS the positive and negative cell populations in $Myf5Cre^{Sor}$, $Pax3^{GFP/+}$, *B195AP-Cre*, and $Pax7^{CreERT2/+}$ constructs (Figure 6). $MyHC^+$ myotubes appeared only in the marker-positive cell fractions (Figures 6A–6C), as confirmed by the relative expression of myogenic genes by qRT-PCR (Figure S5). Of note, $Pax3^+$ dermal precursor cells are detected as GFP^{low} cells in $Pax3^{GFP/+}$ mice (Djian-Zaouche et al., 2012) (Figure 6Da). Dermal GFP^-, GFP^{low}, and GFP^{high} cell fractions of $Pax3^{GFP/+}$ mice were isolated and only the GFP^- cell fraction generated myotubes, with no contribution of dermal precursor (GFP^{low}) cells to the myogenic differentiation (Figures 6Db–6Dd). These data suggested that dermal myogenic precursors derive from $Myf5^+$ $Pax3/Pax7^+$ satellite cells of the PC. To further substantiate this claim, transcriptomic analyses were performed and, once again, the results suggested that dermal myogenic precursor cells were of muscle origin (Figures S6 and S7 and accompanying description).

Ablation of PC Satellite Cells Abrogates Dermis-Derived Myogenesis In Vitro

The previous results strongly suggested that distinct dermal precursors, possibly PC satellite cells, were responsible for dermis-derived myogenesis. To unambiguously demonstrate the origin of dermal myogenic precursors, we specifically ablated PC satellite cells in vivo through crossing the $Pax7^{CreERT2/+}$ construct with $R26R^{GFP\text{-}DTA/+}$ mice (Ivanova et al., 2005). Upon TMX-mediated *Cre* induction (Figure 6E), diphtheria toxin fragment A (DTA) expression is activated in these mice, resulting in specific ablation of the $Pax7^+$ cell lineage. As expected, DTA-mediated ablation of the $Pax7^+$ cells resulted in no $MyHC^+$ myotube formation (Figures 6F–6I). Overall, these results demonstrated

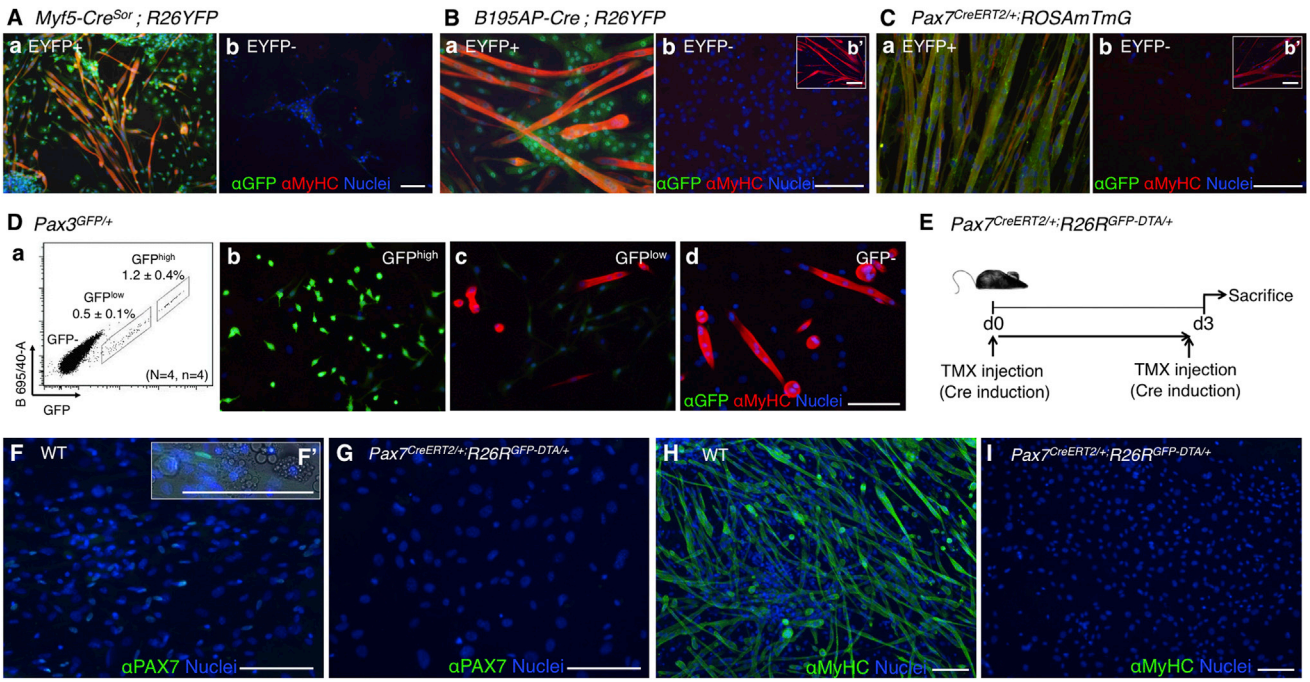

Figure 6. Ablation of Muscle Satellite Cells In Vivo Abrogates In Vitro Dermis-Derived Myotube Formation

(A–C) Contribution of FACS-sorted cell fractions of *Myf5*^{SOR} (A) (EYFP$^+$ [a], EYFP$^-$ [b]), *B195AP* (B) (EYFP$^+$ [a], EYFP$^-$ [b]), and *Pax7*^{CE} (C) (EYFP$^+$ [a], EYFP$^-$ [b]) to striated muscle differentiation was measured by immunofluorescence with anti-GFP (for EYFP expression) and sarcoplasmic anti-myosin heavy-chain (MyHC, all fibers) antibodies.

(D) Flow cytometry analysis of dermal spheres in *Pax3*$^{GFP/+}$ mice (a) showed two distinct cell populations according to GFP expression levels. Data represent mean ± SD (N, mice; n, experiments). (b–d) Contribution of FACS-sorted cell fractions (GFP^{high} [b], GFP^{low} [c], and GFP$^-$ [d]) to striated muscle differentiation was measured by immunofluorescence with anti-GFP and sarcoplasmic anti-myosin heavy-chain (MyHC, all fibers) antibodies.

(E) Outline of experimental design. d, day.

(F–I) Contribution of wild-type (WT) and *Pax7*$^{CE\text{-}DTA}$-derived cells to striated muscle differentiation was measured by immunofluorescence with anti-PAX7 (F and G; higher-magnification inset in F′), and sarcoplasmic anti-myosin heavy-chain (MyHC, all fibers) (H and I) antibodies. Nuclei were counterstained with Hoechst 33258 (blue).

Scale bars, 100 μm. See also Figures S5–S7.

that dermis-derived myogenesis originates from the PC satellite cell population.

In Vivo Contribution of *B195AP*$^+$ Cells to Injury-Induced Skeletal Muscle Regeneration

Dermis-derived precursor cells are able to engraft into injured skeletal muscle (both after freeze-crush injury and cardiotoxin [CTX]-induced damage) and survive up to 20 weeks post injection (Qiu et al., 2010; Wakabayashi et al., 2010). To confirm that *Myf5*$^+$ dermal cells were myogenic in vivo (Figure 7), we injected unsorted dermal cells of the *B195AP-Cre* model crossed with *R26YFP* in the CTX injury model (Figure 7A). One week after injection, one out of three mice injected with *B195AP*$^+$ cells showed 28 ± 3 EYFP$^+$ regenerated myofibers, while in the other two no EYFP$^+$ fiber was detected (Figure 7B and data not shown). Most EYFP$^+$ cells localized in the interstitial spaces of skeletal muscle and a minority was positioned underneath the basement membrane, suggesting repopulation of the satellite cell compartment. Therefore, PC satellite cell-derived *B195AP*$^+$ cells were able to regenerate injured skeletal muscle and thus might represent the in vivo myogenic cell population that had been previously described in the mouse dermis.

DISCUSSION

An important barrier for the use of satellite cells in regenerative medicine, for instance in the field of muscular dystrophies, is the lack of understanding of how to maintain isolated satellite cells in culture such that they are of therapeutic use (Aziz et al., 2012). The PC muscle seems to have high regenerative activity (Brazelton et al., 2003) and is not

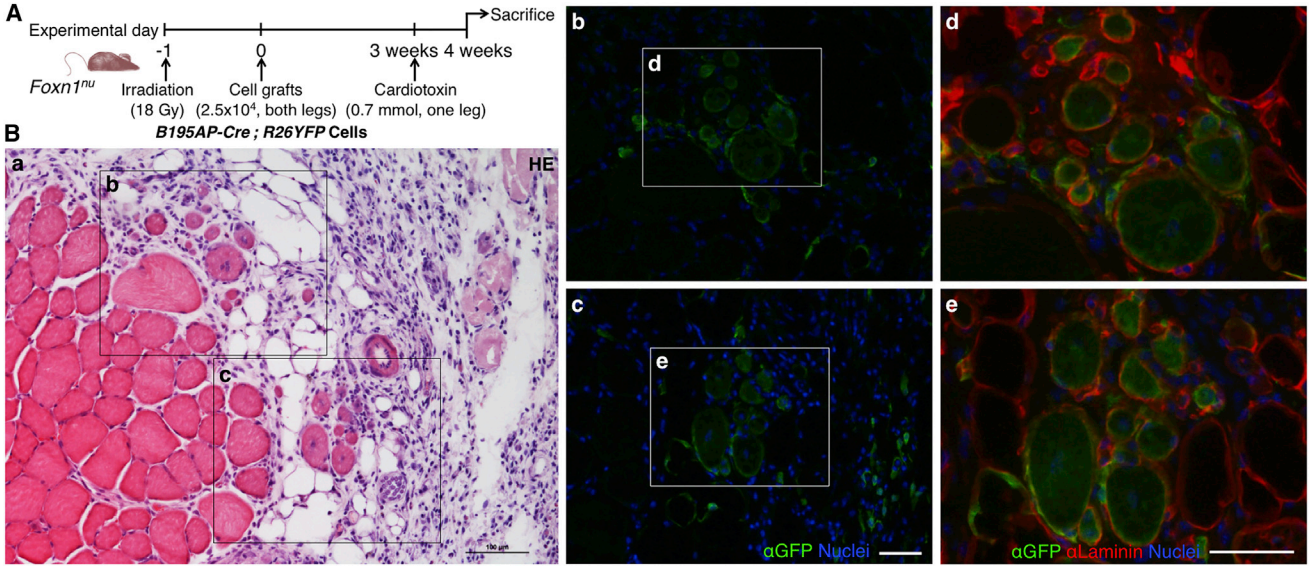

Figure 7. In Vivo Contribution from *B195AP*$^+$ Cells to Striated Muscle Regeneration

(A) Outline of experimental design.

(B) Histological analysis of the in vivo regenerative potential of grafted cells. (a) Tibialis anterior muscle section stained with H&E showing the localization of the other panels. (b and c) Regenerative muscle fibers, defined by centrally located nuclei (blue), showed EYFP expression, as detected with anti-GFP antibody (green). (d and e) Higher-magnification pictures of EYFP$^+$ myofibers (green) and Laminin (red). Nuclei were counterstained with Hoechst 33258 (blue). Scale bars, 100 μm.

only accessible but also dispensable and, as such, can be repeatedly biopsied. For these reasons the PC may be considered as a good muscle for the study of satellite cell biology. In this article we unravel unique aspects of PC muscle biology and describe the origin and role of satellite cells upon skin and muscle wounding.

In response to full-thickness skin wounding, we show an increase in muscle regeneration but no contribution of the *Pax7*-derived cell lineage to the myofibroblasts in the wound bed. This is relevant because a putative role of PC muscle in facilitating the rapid healing (by second intention) observed in rodents has been hypothesized (Greenwood, 2010; Volk and Bohling, 2013). At the wound edge, skNAC, a factor regulating postnatal muscle regeneration (Park et al., 2010), is upregulated in the adjacent PC fibers (Munz et al., 1999), and TAp63$^+$ cells appear in both the PC and newly formed granulation tissue (Bamberger et al., 2005). TAp63 has been linked to dermal stem cell function (Su et al., 2009), and contraction of the granulation tissue supports rapid healing (Billingham and Medawar, 1955; Brunius et al., 1968; Watts et al., 1958). Our lineage-tracing data demonstrate no contribution of *Pax7*$^+$ lineage-derived cells, i.e., activated satellite cells or components of the regenerated myofibers into the granulation tissue, although we cannot discard the contribution from other cell lineages present in PC muscle. In the TA muscle irradiation/CTX model, which is a more standardized muscle injury model, we see that the dermis-derived cells are able to regenerate myofibers, as expected for transplanted satellite cells in such a model.

Previous reports had shown an increased contribution of bone marrow-derived cells (possibly HSCs) to PC muscle (Brazelton et al., 2003; Corbel et al., 2003). This incorporation is unique in that it is highly divergent to other muscle groups (Camargo et al., 2003; Ferrari et al., 1998, 2001; Ferrari and Mavilio, 2002; Sherwood et al., 2004a; Sherwood et al., 2004b; Wagers et al., 2002). However, the donor bone marrow cells, even if able to engraft into the PC satellite cell niche, were unable to generate myotubes from dermis-derived sphere cultures. This may be due to several reasons, but it is tempting to speculate that the engrafted cells failed to reach full conversion to the satellite cell fate, as previously shown in other systems (Cossu, 2004; Lapidos et al., 2004). The relevance of circulating HSC fusion into heart and skeletal muscle are unclear, but the phenomenon keeps arising in the literature (Quijada and Sussman, 2015), and occurs also in human muscle (Stromberg et al., 2013). Based on these results we propose the PC as the most appropriate system to further understand the role of mobilized cells that engraft in skeletal muscle, a research area that has been neglected possibly because of the extreme rarity of the fusion events in the muscle groups that are most often analyzed. Determining the identity of the homing factor(s) that facilitate an

increased engraftment of mobilized cells into the PC in comparison with other skeletal muscles might be exploited for therapeutic use (Asakura, 2012). Potential candidates include the SDF-1/CXCR4 axis (Cheng et al., 2015), although it is important to note that as the PC is signaling for mobilized cell engraftment in the absence of injury, the nature of the signal might be different.

Regarding the developmental origin of PC satellite cells, we have shown that this muscle is no different to other trunk muscles in that it originates from *Myf5*$^{+}$, *Pax3*/*Pax7*$^{+}$ progenitors. This will help in respect of comparability with studies performed in satellite cells from other trunk muscles. Finally, for many years it has been known that a small population of dermal cells, of unknown origin, presents myogenic properties (reviewed by White and Grounds, 2003). Our results unequivocally demonstrate that PC satellite cells are the myogenic precursor cells of murine dermis. The present article and other recent data showing that dermis-derived neural stem cells arise from the Schwann cell lineage (Etxaniz et al., 2014; Gresset et al., 2015) urge us to interpret with caution some of the multipotency wrongly attributed to tissue-resident precursors.

EXPERIMENTAL PROCEDURES

Mouse Strains

Eight-week-old mice were used in all experiments. Strains used are detailed in Table S1. Animal experimentation was approved by Biodonostia Animal Care Committee (San Sebastian, Spain) in accordance with Spanish Royal Decree 53/2013, European Directive 2010/63/EU and other relevant guidelines.

Pax7^{CE}*;ROSAmTmG* Induction by Tamoxifen Injection

Pax7$^{CE/+}$ mice and control (*ROSAmTmG*$^{+/-}$) littermates were intraperitoneally injected (2.5 μL/g mouse) with 20 mg/mL TMX (T5648, Sigma-Aldrich) diluted in corn oil (C8267, Sigma-Aldrich) (Dellavalle et al., 2011), for 3 days at postnatal days 14 (P14), P16, and P35, and euthanized at 7–8 weeks.

Skin Punch

Pax7$^{CreERT2/+}$*;ROSAmTmG* and control *ROSAmTmG* adult mice were intraperitoneally injected with 2 mg TMX for five consecutive days, 4 weeks before injury, or during the first five days of muscle regeneration. Following general anesthesia, the mouse's dorsal skin was shaved and cleaned with povidone and alcohol 70% before proceeding with the skin punch. Full-thickness wounds extended to the depth of the superficial fascia (removing the PC) on either side of the midline were made with a dermal biopsy punch (4 mm diameter; Stiefel) (Wang et al., 2013). By holding the skin with forceps the skin was pushed to one side to avoid damage to back muscles, and two holes were punched simultaneously. The recovered skin was frozen as a control for histological or RNA analysis. The wounds were protected with a sheet of sterile gauze (Tegaderm 4 × 4 cm) kept until the end of the experiment. Buprenorphine painkiller (Vetergesic 0.3 mg/mL; Soceval) was injected directly after the surgery and again 4–6 hr later, and on the next day. Mice were placed individually in cages allowing free access to food and water ad libitum. After wounding, animals were carefully monitored to avoid infection and suffering. Skins were finally recovered 5 and 10 days after injury. As controls, uninjured skins from the same animals were taken (n = 3 animals per condition).

Isolation, Proliferation, and Striated Muscle Differentiation of Dermal Precursor Cells

Precursor cells were isolated from dorsal back skin and imaged by fluorescence as described by García-Parra et al. (2012). Dermal sphere expansion was performed in proliferation medium (Neurobasal A [Gibco] supplemented with 2% B27 [Gibco], 200 mM 1% L-glutamine [Sigma-Aldrich], and 1% penicillin/streptomycin, supplemented with 2% low serum growth supplement [Gibco], 40 ng/mL epidermal growth factor [R&D Systems], and 80 ng/mL basic fibroblast growth factor [FGF2; R&D]). For differentiation, extracellular matrix-coated glass coverslips were prepared as described by Garcia-Parra et al. (2014). Primary spheres were gently disaggregated with a 0.25% trypsin-EDTA solution (Sigma-Aldrich) and resuspended in proliferation medium without added growth factors plus 10% fetal bovine serum (ATCC), before plating onto coated coverslips at a density of 80,000 cells/cm^2. Every 2 days, half of the medium was replenished.

Depletion of Dermal Satellite Cells

Pax7$^{CreERT2/+}$*;R26R*$^{GFP\text{-}DTA/+}$ and control *R26R*$^{GFP\text{-}DTA/+}$ mice were intraperitoneally injected with 10 mg TMX as previously described (Lepper et al., 2011). Forty-eight hours later, dorsal skins were recovered for sphere culture, and TA and soleus muscles frozen for histological and RNA analysis (n = 3 animals per condition).

In Vivo Cell Grafting and Muscle Injury

Primary dermospheres at day 7 of proliferation were gently disaggregated with a 0.25% trypsin-EDTA solution (Sigma-Aldrich) and resuspended in PBS. Muscle damage experiments were done according to Boldrin et al. (2012) and Boldrin et al. (2009). Ten-week-old nude *Foxn1*^{nu} mice were anesthetized and both hind limbs were irradiated with 18 Gy at a dose rate of 300 cGy/min. One day later, mice were anesthetized with isoflurane and received 2.5 × 10^4 unsorted *Myf5Cre*^{SOR}*;R26YFP* (pooled from n = 3 mice) or *B195AP-Cre;R26YFP* (n = 3 mice) cells into both TA muscles using a 26-gauge Hamilton syringe. Three weeks after transplantation, right TA muscles of anesthetized host mice were injected with 0.7 mmol cardiotoxin (Sigma, C9759) while PBS was administered to the contralateral muscle. Controls were age-matched mice that were non-irradiated and received PBS. Engrafted muscles were removed 4 weeks after cell injection and processed for histological analysis. Seven-micrometer serial transverse cryosections were cut at intervals of 100 μm throughout the entire muscles. Sections were stained with H&E and by immunofluorescence staining using antibodies as detailed in Supplemental Experimental Procedures. The mean number of donor origin regenerated myofibers was

calculated by counting the number of EYFP$^+$ centrally nucleated fibers in three intervals of 100-μm serial sections.

Assessment of Statistical Significance

Statistical analysis was conducted using GraphPad Prism software. A one-way ANOVA with subsequent pairwise multiple comparison procedures (Bonferroni's test) was used to assess statistical significance of the results from qRT-PCR experiments. Student's t test was used to assess statistical significance of the results from *Pax7*(GFP)$^+$ cell quantification experiments. Asterisks in figures represent statistical significance of *$p < 0.05$, **$p < 0.01$, or ***$p < 0.001$.

ACCESSION NUMBERS

Transcriptomic data of dermal cell fractions are deposited in NCBI's Gene Expression Omnibus (Edgar et al., 2002) under accession number GEO: GSE67693.

SUPPLEMENTAL INFORMATION

Supplemental Information includes Supplemental Results, Supplemental Experimental Procedures, seven figures, and two tables and can be found with this article online at http://dx.doi.org/10.1016/j.stemcr.2016.08.002.

AUTHOR CONTRIBUTIONS

N.N.G. performed most of the experimental work, with the help of M.G., J.L., and P.G.P. C.S.J. helped perform in vivo cell transplantation experiments. S.A.M. and F.R. were responsible for inducible *Pax7* lineage-tracing experiments. A.A. performed qRT-PCR analyses. J.J.C. generated *B195AP-Cre*-expressing mice and together with M.L.M. characterized this transgenic line. P.G.B. and J.M.G.V. performed ultrastructural analyses. L.T., V.A.L., and M.J.A.B. did the transcriptomics and their corresponding analyses, respectively. D.H. and A.B. performed bone marrow transplantation experiments. A.M. and A.L.M. provided helpful guidance, reagents, and suggestions. N.N.G. and A.I. wrote the manuscript, which was approved by all authors prior to submission. P.G.P. and A.I. directed all experimental work.

ACKNOWLEDGMENTS

We thank investigators for monoclonal antibodies A4.1025 (H.M. Blau) and F5D (W.E. Wright), which were obtained from the Developmental Studies Hybridoma Bank (developed under the auspices of the NICHD and maintained by The University of Iowa, Department of Biology, Iowa City, IA). Special thanks to G. Cossu for critical reading of the manuscript. We are also grateful to F. Costantini, C.-M. Fan, C. Lepper, M.J. Sánchez-Sanz, H. Sakai, and S. Tajbakhsh for kindly providing study materials; S. Lamarre of the GeT-Biochip facility for help in the microarray data; D. Ortiz de Urbina, J.C. Mazabuel, and A. Guisasola for help with irradiation protocol; and A. Aduriz, A. Pavón, and M. P. López-Mato for help with FACS analyses. This work was supported by grants from Instituto de Salud Carlos III (ISCIII; PS09/00660, PI13/02172, and PI14/7436), Gobierno Vasco (SAIO12-PE12BN008) from Spain and the European Union (POCTEFA-INTERREG IV A program; REFBIO13/BIOD/006 and REFBIO13/BIOD/009). N.N.G. received a studentship from the Department of Education, University and Research of the Basque Government (PRE2013-1-1168). P.G.P. received fellowships from the Department of Health of the Basque government (2013011016), EMBO (Short-Term; ASTF 542–2013), and Boehringer Ingelheim Fonds. M.L.M. and J.J.C. were supported by a Marie Curie Career Integration Grant from the European Commission (PEOPLE-CIG/1590). A.I. was supported by the Programa I3SNS (CES09/015) from ISCIII and by Osakidetza-Servicio Vasco de Salud (Spain). M.G. and S.A.M. contributed equally to this work.

Received: April 7, 2015
Revised: August 1, 2016
Accepted: August 1, 2016
Published: September 1, 2016

REFERENCES

Asakura, A. (2012). Skeletal muscle-derived hematopoietic stem cells: muscular dystrophy therapy by bone marrow transplantation. J. Stem Cell Res Ther. (*Suppl 11*), 005.

Atit, R., Sgaier, S.K., Mohamed, O.A., Taketo, M.M., Dufort, D., Joyner, A.L., Niswander, L., and Conlon, R.A. (2006). Beta-catenin activation is necessary and sufficient to specify the dorsal dermal fate in the mouse. Dev. Biol. *296*, 164–176.

Aziz, A., Sebastian, S., and Dilworth, F.J. (2012). The origin and fate of muscle satellite cells. Stem Cell Rev. *8*, 609–622.

Bamberger, C., Hafner, A., Schmale, H., and Werner, S. (2005). Expression of different p63 variants in healing skin wounds suggests a role of p63 in reepithelialization and muscle repair. Wound Repair Regen. *13*, 41–50.

Billingham, R.E., and Medawar, P.B. (1955). Contracture and intussusceptive growth in the healing of extensive wounds in mammalian skin. J. Anat. *89*, 114–123.

Biressi, S., Bjornson, C.R., Carlig, P.M., Nishijo, K., Keller, C., and Rando, T.A. (2013). Myf5 expression during fetal myogenesis defines the developmental progenitors of adult satellite cells. Dev. Biol. *379*, 195–207.

Boldrin, L., Zammit, P.S., Muntoni, F., and Morgan, J.E. (2009). Mature adult dystrophic mouse muscle environment does not impede efficient engrafted satellite cell regeneration and self-renewal. Stem Cells *27*, 2478–2487.

Boldrin, L., Neal, A., Zammit, P.S., Muntoni, F., and Morgan, J.E. (2012). Donor satellite cell engraftment is significantly augmented when the host niche is preserved and endogenous satellite cells are incapacitated. Stem Cells *30*, 1971–1984.

Brazelton, R., Nystrom, M., and Blau, H. (2003). Significant differences among skeletal muscles in the incorporation of bone marrow-derived cells. Dev. Biol. *262*, 64–74.

Brunius, U., Zederfeldt, B., and Ahren, C. (1968). Healing of skin incisions with intact subcutaneous muscle closed by non-suture technique. A tensiometric and histologic study in the rat. Acta Chir. Scand. *134*, 187–193.

Buckingham, M., and Rigby, P.W.J. (2014). Gene regulatory networks and transcriptional mechanisms that control myogenesis. Dev. Cell *28*, 225–238.

Camargo, F.D., Green, R., Capetanaki, Y., Jackson, K.A., and Goodell, M.A. (2003). Single hematopoietic stem cells generate skeletal muscle through myeloid intermediates. Nat. Med. *9*, 1520–1527.

Carvajal, J.J., Cox, D., Summerbell, D., and Rigby, P.W.J. (2001). A BAC transgenic analysis of the Mrf4/Myf5 locus reveals interdigitated elements that control activation and maintenance of gene expression during muscle development. Development *1868*, 1857–1868.

Cheng, M., Huang, K., Zhou, J., Yan, D., Tang, Y.L., Zhao, T.C., Miller, R.J., Kishore, R., Losordo, D.W., and Qin, G. (2015). A critical role of Src family kinase in SDF-1/CXCR4-mediated bone-marrow progenitor cell recruitment to the ischemic heart. J. Mol. Cell Cardiol. *81*, 49–53.

Corbel, S.Y., Lee, A., Yi, L., Duenas, J., Brazelton, T.R., Blau, H.M., and Rossi, F.M. (2003). Contribution of hematopoietic stem cells to skeletal muscle. Nat. Med. *9*, 1528–1532.

Cossu, G. (2004). Fusion of bone marrow-derived stem cells with striated muscle may not be sufficient to activate muscle genes. J. Clin. Invest. *114*, 1540–1543.

Dellavalle, A., Maroli, G., Covarello, D., Azzoni, E., Innocenzi, A., Perani, L., Antonini, S., Sambasivan, R., Brunelli, S., Tajbakhsh, S., et al. (2011). Pericytes resident in postnatal skeletal muscle differentiate into muscle fibres and generate satellite cells. Nat. Commun. *2*, 499.

DiMario, J.X., Uzman, A., and Strohman, R.C. (1991). Fiber regeneration is not persistent in dystrophic (MDX) mouse skeletal muscle. Dev. Biol. *148*, 314–321.

Djian-Zaouche, J., Campagne, C., Reyes-Gomez, E., Gadin-Czerw, S., Bernex, F., Louise, A., Relaix, F., Buckingham, M., Panthier, J.J., and Aubin-Houzelstein, G. (2012). Pax3(GFP), a new reporter for the melanocyte lineage, highlights novel aspects of PAX3 expression in the skin. Pigment Cell Melanoma Res. *25*, 545–554.

Edgar, R., Domrachev, M., and Lash, A.E. (2002). Gene Expression Omnibus: NCBI gene expression and hybridization array data repository. Nucleic Acids Res. *30*, 207–210.

Eppig, J.T., Blake, J.A., Bult, C.J., Kadin, J.A., and Richardson, J.E. (2015). The Mouse Genome Database (MGD): facilitating mouse as a model for human biology and disease. Nucleic Acids Res. *43*, D726–D736.

Etxaniz, U., Perez-San Vicente, A., Gago-Lopez, N., Garcia-Dominguez, M., Iribar, H., Aduriz, A., Perez-Lopez, V., Burgoa, I., Irizar, H., Munoz-Culla, M., et al. (2014). Neural-competent cells of adult human dermis belong to the Schwann lineage. Stem Cell Rep. *3*, 774–788.

Ferrari, G., and Mavilio, F. (2002). Myogenic stem cells from the bone marrow: a therapeutic alternative for muscular dystrophy? Neuromuscul. Disord. *12* (*Suppl 1*), S7–S10.

Ferrari, G., Cusella-De Angelis, G., Coletta, M., Paolucci, E., Stornaiuolo, A., Cossu, G., and Mavilio, F. (1998). Muscle regeneration by bone marrow-derived myogenic progenitors. Science *279*, 1528–1530.

Ferrari, G., Stornaiuolo, A., and Mavilio, F. (2001). Failure to correct murine muscular dystrophy. Nature *411*, 1014–1015.

García-Parra, P., Cavaliere, F., Maroto, M., Bilbao, L., Obieta, I., López de Munain, A., Alava, J.I., and Izeta, A. (2012). Modeling neural differentiation on micropatterned substrates coated with neural matrix components. Front. Cell Neurosci. *6*, 10.

Garcia-Parra, P., Naldaiz-Gastesi, N., Maroto, M., Padin, J.F., Goicoechea, M., Aiastui, A., Fernandez-Morales, J.C., Garcia-Belda, P., Lacalle, J., Alava, J.I., et al. (2014). Murine muscle engineered from dermal precursors: an in vitro model for skeletal muscle generation, degeneration, and fatty infiltration. Tissue Eng. Part C Methods *20*, 28–41.

Gayraud-Morel, B., Chretien, F., Jory, A., Sambasivan, R., Negroni, E., Flamant, P., Soubigou, G., Coppee, J.Y., Di Santo, J., Cumano, A., et al. (2012). Myf5 haploinsufficiency reveals distinct cell fate potentials for adult skeletal muscle stem cells. J. Cell Sci. *125*, 1738–1749.

Greenwood, J.E. (2010). Function of the panniculus carnosus—a hypothesis. Vet. Rec. *167*, 760.

Gresset, A., Coulpier, F., Gerschenfeld, G., Jourdon, A., Matesic, G., Richard, L., Vallat, J.M., Charnay, P., and Topilko, P. (2015). Boundary caps give rise to neurogenic stem cells and terminal glia in the skin. Stem Cell Rep. *5*, 278–290.

Gros, J., Manceau, M., Thome, V., and Marcelle, C. (2005). A common somitic origin for embryonic muscle progenitors and satellite cells. Nature *435*, 954–958.

Hughes, A.F.W., and Dann, L. (1941). Vascular regeneration in experimental wounds and burns. Br. J. Exp. Pathol. *22*, 9–14.

Ivanova, A., Signore, M., Caro, N., Greene, N.D., Copp, A.J., and Martinez-Barbera, J.P. (2005). In vivo genetic ablation by Cre-mediated expression of diphtheria toxin fragment A. Genesis *43*, 129–135.

Kassar-Duchossoy, L., Gayraud-Morel, B., Gomes, D., Rocancourt, D., Buckingham, M., Shinin, V., and Tajbakhsh, S. (2004). Mrf4 determines skeletal muscle identity in Myf5:Myod double-mutant mice. Nature *431*, 466–471.

Kassar-Duchossoy, L., Giacone, E., Gayraud-Morel, B., Jory, A., Gomès, D., and Tajbakhsh, S. (2005). Pax3/Pax7 mark a novel population of primitive myogenic cells during development. Genes Dev. *19*, 1426–1431.

Kuang, S., Kuroda, K., Grand, F.L., and Rudnicki, M. (2007). Asymmetric self-renewal and commitment of satellite stem cells in muscle. Cell *129*, 999–1010.

Lapidos, K.A., Chen, Y.E., Earley, J.U., Heydemann, A., Huber, J.M., Chien, M., Ma, A., and McNally, E.M. (2004). Transplanted hematopoietic stem cells demonstrate impaired sarcoglycan expression after engraftment into cardiac and skeletal muscle. J. Clin. Invest. *114*, 1577–1585.

Lepper, C., and Fan, C.-m. (2011). Inducible lineage tracing of Pax7-descendant cells reveals embryonic origin of adult satellite cells. Genesis *48*, 424–436.

Lepper, C., Partridge, T.a., and Fan, C.-M. (2011). An absolute requirement for Pax7-positive satellite cells in acute injury-induced skeletal muscle regeneration. Development *138*, 3639–3646.

Mauro, A. (1961). Satellite cell of skeletal muscle fibers. J. Biophys. Biochem. Cytol. *9*, 493–495.

McDonald, T.A., Zepeda, M.L., Tomlinson, M.J., Bee, W.H., and Ivens, I.A. (2010). Subcutaneous administration of biotherapeutics: current experience in animal models. Curr. Opin. Mol. Ther. *12*, 461–470.

Munz, B., Wiedmann, M., Lochmuller, H., and Werner, S. (1999). Cloning of novel injury-regulated genes. Implications for an important role of the muscle-specific protein skNAC in muscle repair. J. Biol. Chem. *274*, 13305–13310.

Nag, A.C., and Foster, J.D. (1981). Myogenesis in adult mammalian skeletal muscle in vitro. J. Anat. *132*, 1–18.

Novakov, S.S., Yotova, N.I., Petleshkova, T.D., and Muletarov, S.M. (2008). Sternalis muscle—a riddle that still awaits an answer short communication. Folia Med. *50*, 63–66.

Park, C.Y., Pierce, S.A., von Drehle, M., Ivey, K.N., Morgan, J.A., Blau, H.M., and Srivastava, D. (2010). skNAC, a Smyd1-interacting transcription factor, is involved in cardiac development and skeletal muscle growth and regeneration. Proc. Natl. Acad. Sci. USA *107*, 20750–20755.

Qiu, Z., Miao, C., Li, J., Lei, X., Liu, S., Guo, W., Cao, Y., and Duan, E.K. (2010). Skeletal myogenic potential of mouse skin-derived precursors. Stem Cells Dev. *19*, 259–268.

Quijada, P., and Sussman, M.A. (2015). Circulating around the tissue: hematopoietic cell-based fusion versus transdifferentiation. Circ. Res. *116*, 563–565.

Randolph, M.E., and Pavlath, G.K. (2015). A muscle stem cell for every muscle: variability of satellite cell biology among different muscle groups. Front. Aging Neurosci. *7*, 190.

Relaix, F., Rocancourt, D., Mansouri, A., and Buckingham, M. (2005). A Pax3/Pax7-dependent population of skeletal muscle progenitor cells. Nature *435*, 948–953.

Robson, L.G., Di Foggia, V., Radunovic, A., Bird, K., Zhang, X., and Marino, S. (2011). Bmi1 is expressed in postnatal myogenic satellite cells, controls their maintenance and plays an essential role in repeated muscle regeneration. PLoS One *6*, e27116.

Sarig, R., Baruchi, Z., Fuchs, O., Nudel, U., and Yaffe, D. (2006). Regeneration and transdifferentiation potential of muscle-derived stem cells propagated as myospheres. Stem Cells *24*, 1769–1778.

Schiaffino, S., Rossi, A.C., Smerdu, V., Leinwand, L.A., and Reggiani, C. (2015). Developmental myosins: expression patterns and functional significance. Skeletal Muscle *5*, 22.

Schienda, J., Engleka, K.A., Jun, S., Hansen, M.S., Epstein, J.A., Tabin, C.J., Kunkel, L.M., and Kardon, G. (2006). Somitic origin of limb muscle satellite and side population cells. Proc. Natl. Acad. Sci. USA *103*, 945–950.

Sherwood, R.I., Christensen, J.L., Conboy, I.M., Conboy, M.J., Rando, T.A., Weissman, I.L., and Wagers, A.J. (2004a). Isolation of adult mouse myogenic progenitors: functional heterogeneity of cells within and engrafting skeletal muscle. Cell *119*, 543–554.

Sherwood, R.I., Christensen, J.L., Weissman, I.L., and Wagers, A.J. (2004b). Determinants of skeletal muscle contributions from circulating cells, bone marrow cells, and hematopoietic stem cells. Stem Cells *22*, 1292–1304.

Stromberg, A., Jansson, M., Fischer, H., Rullman, E., Hagglund, H., and Gustafsson, T. (2013). Bone marrow derived cells in adult skeletal muscle tissue in humans. Skeletal Muscle *3*, 12.

Su, X., Paris, M., Gi, Y.J., Tsai, K.Y., Cho, M.S., Lin, Y.L., Biernaskie, J.A., Sinha, S., Prives, C., Pevny, L.H., et al. (2009). TAp63 prevents premature aging by promoting adult stem cell maintenance. Cell Stem Cell *5*, 64–75.

Valiente-Alandi, I., Albo-Castellanos, C., Herrero, D., Arza, E., Garcia-Gomez, M., Segovia, J.C., Capecchi, M., and Bernad, A. (2015). Cardiac Bmi1(+) cells contribute to myocardial renewal in the murine adult heart. Stem Cell Res. Ther. *6*, 205.

Volk, S.W., and Bohling, M.W. (2013). Comparative wound healing–are the small animal veterinarian's clinical patients an improved translational model for human wound healing research? Wound Repair Regen. *21*, 372–381.

Wagers, A.J., Sherwood, R.I., Christensen, J.L., and Weissman, I.L. (2002). Little evidence for developmental plasticity of adult hematopoietic stem cells. Science *297*, 2256–2259.

Wakabayashi, M., Ito, Y., Hamazaki, T.S., and Okochi, H. (2010). Efficient myogenic differentiation of murine dermal Sca-1 (-) cells via initial aggregation culture. Tissue Eng. *16*, 3251–3259.

Wang, X., Ge, J., Tredget, E.E., and Wu, Y. (2013). The mouse excisional wound splinting model, including applications for stem cell transplantation. Nat. Protoc. *8*, 302–309.

Watts, G.T., Grillo, H.C., and Gross, J. (1958). Studies in wound healing: II. The role of granulation tissue in contraction. Ann. Surg. *148*, 153–160.

White, J.D., and Grounds, M.D. (2003). Harnessing the therapeutic potential of myogenic stem cells. Cytotechnology *41*, 153–164.

Wojciechowicz, K., Gledhill, K., Ambler, C.A., Manning, C.B., and Jahoda, C.A. (2013). Development of the mouse dermal adipose layer occurs independently of subcutaneous adipose tissue and is marked by restricted early expression of FABP4. PLoS One *8*, e59811.

Stem Cell Reports, Volume *7*

Supplemental Information

Identification and Characterization of the Dermal Panniculus Carnosus Muscle Stem Cells

Neia Naldaiz-Gastesi, María Goicoechea, Sonia Alonso-Martín, Ana Aiastui, Macarena López-Mayorga, Paula García-Belda, Jaione Lacalle, Carlos San José, Marcos J. Araúzo-Bravo, Lidwine Trouilh, Véronique Anton-Leberre, Diego Herrero, Ander Matheu, Antonio Bernad, José Manuel García-Verdugo, Jaime J. Carvajal, Frédéric Relaix, Adolfo Lopez de Munain, Patricia García-Parra, and Ander Izeta

SUPPLEMENTAL RESULTS

Transcriptomic analyses confirm the myogenic identity of *Myf5+* dermal precursor cells. To understand if myogenic precursors arise during dermal sphere culture or where otherwise present in the original dissociated tissue sample, transcriptomic analyses were performed in *Myf5*^{Sor} positive cell-derived sphere cultures and the appearance of myogenic genes at day 7 of proliferation culture as compared to day 0 was analyzed (Figure S6). A principal component analysis (PCA) of gene expression data of 78 arrays corresponding to 35 cell different populations (as detailed in Table S2) showed that all dermis-derived samples (myogenic and non-myogenic) clustered together with known myogenic samples but also with fibroblasts and adipocytes (Figure S6A). Pairwise comparisons showed that, of the 4,735 genes differentially expressed between these samples, 52 probes (15 genes) were associated with the GO category "Satellite Cell" and 154 probes (63 genes) classified under "Striated Muscle Cell Differentiation". Analyses of these myogenic probes/genes showed that activated satellite/immature myoblast markers such as *Musk* (DeChiara et al., 1996), *Myod1*, *Shh* (Voronova et al., 2013), *Igfbp5* (Sharples et al., 2011) and *Bmp4* (Dahlqvist et al., 2003; Ono et al., 2011) were preferentially expressed at day 0 sphere cultures. In contrast, committed/differentiated myoblast genes such as *Cdh2* (Lovett et al., 2006), *Rara/Rarb* (Halevy and Lerman, 1993), *Myh3*, *Kcnh1* (Rozwadowska et al., 2013; Stern-Straeter et al., 2009) and *Myf6* (Sambasivan et al., 2013) were upregulated at day 7 (Figure S6, B-C). These data suggested that activated PC satellite cells were expanding and differentiating in dermal sphere cultures.

Dermal myogenic fractions branched together and separate from non-myogenic (*Cspg4+*) fraction when hierarchical clustering of samples was performed using the correlation metric and the average linkage method (Figure S7A). To further discriminate, differentially expressed genes with a FC>2 in a log2 scale between myogenic and non-myogenic (*Cspg4+*) dermal samples were determined. As expected, key myogenic factors such as *Myod1, Myf6, Ttn* and *Myog* were downregulated in the dermal non-myogenic fraction (*Cspg4+*) when compared to the dermal myogenic fractions (Figure S7B). Furthermore, of the 1,476-3,397 genes upregulated when compared to *Cspg4+* dermal cells, the dermal myogenic and other myogenic samples obtained from public databases shared 1,000 genes (Figure S7C). Finally, gene set enrichment analysis (GSEA) of molecular signatures showed two muscle development categories among the significant GSEA-enriched terms (Figure S7D). In all, transcriptomic data are compatible with dermal myogenic precursor cells being of muscle origin.

SUPPLEMENTAL MATERIALS AND METHODS

Generation of the new *B195AP-Cre* line. The *B195APZ* BAC construct was modified by recombineering (Swaminathan et al., 2001) with modifications as described previously (Carvajal et al., 2008). BAC clones were transferred into DY380 cells (kindly provided by Neil Copeland, National Cancer Institute-Frederick, Frederick, Maryland), which carry the temperature-inducible lambda-recombinase system. Briefly, 250bp homology arms were generated by PCR and joined to *Cre*. The construct was electroporated into electrocompetent DY380 cells carrying the *B195APZ* construct and used to replace the *nlacZ* gene by the *Cre* gene. Pools of 20-30 clones were screened by PCR and positive pools further diluted to single cells in order to identify correctly targeted clones. Full details on the targeting constructs can be obtained on request. BAC DNA was prepared using the QIAgen Maxiprep kit (Qiagen) as described previously (Carvajal et al., 2001), dialyzed against BAC microinjection buffer (10 mM Tris-HCl pH 7.5, 0.1 mM EDTA pH 8.0, 100mM NaCl), diluted to 1.6 ng/ml in BAC microinjection buffer and used to inject day 0 fertilized mouse eggs from CBA/Ca × C57Bl/6 crosses. For the generation of this new line, experimentation was performed according to United Kingdom Home Office Regulations and current Spanish legislation (RD53/2013) on animal experimentation.

Skin histology for inmunofluorescence. Murine dorsal skin fragments of approximately 0.5 cm2 were excised, and were directly embedded in OCT (Sakura) and frozen in isopentane (Merck) cooled in liquid nitrogen or pre-fixed in fixative solution (Histofix; Histolab) at 4ºC overnight. Fixed samples were immersed in 5% sucrose at 4ºC for 5 hours and in 30% sucrose at 4ºC overnight. The next day, samples were embedded in OCT, and immediately frozen in isopentane cooled in liquid nitrogen. Seven µm cryostat transverse sections were fixed in cold methanol for 3 min or in 4% paraformaldehyde 10 min, incubated in 0,1% Triton in PBS for 20 minutes, and followed by 10% goat serum for 30 min or with 10% BSA solution 1 hour. Primary antibodies were incubated for 1h at RT or O/N at 4ºC, and then incubated with secondary antibodies (see supplementary data) for 1h at RT. The samples were stained with Hoechst, washed 3 times with phosphate buffered saline (PBS) and once with distilled water and with milliQ water, and then mounted with Fluoro-Gel (Electron Microscopy Sciences). The samples were examined under epifluorescence microscope (Eclipse TS100) or Zeiss LSM 510 Meta confocal microscope.

Immunofluorescence and microscopy. Cells were fixed in 4% paraformaldehyde (PFA; Electron Microscopy Sciences) for 10 min at room temperature (RT) and then they were permeabilized/blocked by using 0.3% Triton X-100 in PBS (PBST) plus 5% normal donkey serum (Sigma-Aldrich) for 1h at RT. Cells were incubated with the appropriate primary antibody diluted in PBST for 2h at RT (as detailed below). After that, cells were incubated for 1h at RT with the appropriate secondary antibody diluted in PBST (detailed in Supplementary data). Prior to mounting in Vectashield (Vector Laboratories), cells were counterstained with 10 µg/ml Hoechst 33258 (Sigma-Aldrich) for 2 min at RT. Fluorescence images were obtained by using a Nikon Eclipse 80i microscope coupled to Nikon Digital Sight and analyzed with Nikon NIS-Elements Advance Research software. Primary antibodies used were anti-myogenin (Myog) (F5D; 1:50; Developmental Studies Hybridoma Bank, DSHB), anti-myosin heavy chain (MyHC) (A4.1025, all fibers; 1:50; DSHB), goat anti-GFP (GFP) (ab6673; 1:500; Abcam), chicken anti-GFP (GFP) (ab13970; 1:500; Abcam), anti-DsRed (DsRed) (632496; 1:100; Clontech) and anti-Laminin (L9393, Sigma-Aldrich). Secondary antibodies used were donkey anti-goat Alexa Fluor 488 (A11055; 1:500; Invitrogen), donkey anti-mouse Alexa Fluor 555 (A31570; 1:500; Invitrogen), donkey anti-rabbit Alexa Fluor 555 (A31572; 1:500; Invitrogen), Alexa fluor 594-conjugated goat anti-rabbit (A11012) and goat anti-chicken DyLight® 488 (ab96947; 1:500; Abcam).

Transmission electron microscopy (TEM). After fixation in 3.5% glutaraldehyde (Electron Microscopy Sciences), cell cultures were washed in 0.1 M PBS (pH 7.4) and treated with 2% osmium tetraoxide (Electron Microscopy Sciences) in 0.1 M PBS (pH 7,4) for 2h at RT. Samples were rinsed, dehydrated through increasing ethanol solutions and stained in 2% uranyl acetate (Electron Microscopy Sciences) at 70% ethanol. Dehydrated cell cultures were embedded in araldite (Fluka). Semithin sections (1.5µm-thick) were cut with a diamond knife and stained with 1% toluidine blue solution (Sigma-Aldrich), re-embedded for ultrathin (70 nm-thick) sectioning, and examined under a Tecnai-Spirit Electron Transmission Microscope (TEM) coupled to a Morada TEM CCD camera (Soft Imaging System).

β-Galactosidase reporter gene staining and Alkaline Phosphatase reporter gene staining. LacZ staining was performed using the β-Galactosidase Reporter Gene Staining Kit (GALS; Sigma-Aldrich). Skin fragments were fixed in 4% paraformaldehide (PFA) for 40 min at 4°C. After

incubation in X-gal solution for 3h at 37°C, samples were washed, dehydrated with increasing sucrose concentration (10-20%) for 3 hours, embedded in OCT and frozen in liquid nitrogen-cooled isopentane (Merck). Sixty cryostat sections were cut, mounted in glycerol and examined under the microscope. Alkaline Phosphatase (AP) reporter gene staining was performed using the Alkaline Phosphatase Blue Membrane Substrate Solution (AB0300-1KT; Sigma-Aldrich). Skin fragments were fixed in 4% paraformaldehyde in PBS O/N at 4°C, rinsed twice in PBS supplemented with 2 mM MgCl2 (PBSMg), and washed in PBSMg for 10 minutes. Endogenous phosphatases were inactivated by incubation for 1 hour in PBSMg at 65°C. Samples were washed in ice-cold AP-buffer (100 mM Tris-HCl pH 9.5, 100 mM NaCl, 50 mM MgCl2, 0.1% Tween 20) and AP-buffer, transferred to AP-staining buffer and stained for 40 min in the dark at 4°C. The reaction was stopped by washing the tissue samples in ice-cold PBS in the dark at 4°C for 16 hours, dehydrated with increasing sucrose concentration (10-20%) for 3 hours, embedded in OCT and frozen as above. Sixty cryostat sections were cut, mounted in glycerol and examined under the microscope. For β-Galactosidase staining on whole-mount mouse embryos, these were fixed overnight in Mirsky's fixative (National Diagnostics) at 4°C, washed three times in PBSA (Ca++, Mg++-free phosphate-buffered saline)/0.02% Nonidet P-40 for 20 min at room temperature, placed in 7-10 ml of X-gal solution [5 mM K3Fe(CN)6, 5 mM K4Fe(CN)6 • 3H2O, 2 mM MgCl2, 0.02% Nonidet P-40, 0.4 mg/ml X-Gal in PBSA] for 2–6 h (depending on stage) at 37°C, and post-fixed in Mirsky's fixative.

Flow cytometry and cell sorting. Cultured spheres were dissociated with 0.25% Trypsin-EDTA (Sigma) for 5 min at 37ºC, PBS-washed, filtered through a 70 µm cell strainer, counted, and resuspended in PBS without Ca^{++} and Mg^{++}, with BSA 0.5%, 25mM HEPES and 5mM EDTA (sorting buffer; pH=7.2). For flow cytometry assays of YFP, data were acquired on a BD FACSCantoA flow cytometer using blue excitation and collecting fluorescent signals on the 530/30 (YFP) band pass filter. Tomato and GFP expression data were acquired on BD FACSAria III cell sorter using blue and yellow-green excitation and collecting fluorescent signals on the 530/30 (GFP) and 610/20 (TdTomato) band pass filters. Data acquisition was done for both assays with FACSDiva Software using control littermate mice to adjust setting parameters. Sample data were analyzed excluding doublets and non-viable cells (To-Pro-3 positive cells), with BD FACS diva software and FlowJo. Data are represented as dot plots showing green fluorescence (EYFP or EGFP) vs. orange fluorescence (autofluorescence).

Syndecan-4-based cell sorting. Cultured dermospheres were pelleted and dissociated with 0.25% Trypsin-EDTA (Sigma) for 5 min at 37°C, PBS-washed, filtered through a 70 µm cell strainer, and counted. Cells were blocked with PBS with BSA 1% and FBS 10% for 10 min at room temperature. The primary antibody, Biotin Rat Anti-Mouse Syndecan-4 (IgG2a) (550351; 1µg/test; BD Biosciences), and isotype, Biotin Rat IgG2a,κ Isotype Control (553928; 1µg/test; BD Biosciences) were added and incubated for 30 min at 4ºC. The cells were washed with PBS with BSA 1%, incubated with APC Streptavidin (554067; 0.2mg/ml; BD Biosciences) for 30 min at 4ºC, washed again, and re-suspended in PBS without Ca^{++} and Mg^{++}, with BSA 0.5%, 25mM HEPES and 5mM EDTA (sorting buffer; pH=7.2) onto 5 ml polypropylene tubes. Auto-fluorescence was adjusted with the *wt* mice. PMT settings were established on live singlets by using unstained cells. Non-specific bindings were evaluated with the corresponding isotypic controls used at the same concentration, same isotype and same fluorophore that the antibody of interest. Sorting experiments were done on a FACSAria III cell sorter (BD Biosciences), at low sheath pressure (20 psi) using 100 µm nozzle. Sorting procedures were done excluding dead cells (with either 7AAD or Sytox Green) and doublets; sorted cells were collected on proliferation medium without serum.

Gene expression. Total RNA was extracted from cells by miRNeasy Mini kit (Qiagen) and converted into complementary DNA with the High-Capacity cDNA Reverse Transcription Kit (Applied Biosystems). Real-time quantitative PCR (qRT-PCR) analysis was carried out using Taqman gene expression assays in the 7900 HT Fast Real-Time PCR System (Applied Biosystems). Each cDNA sample was amplified in triplicates. The cycling conditions were 95ºC/10 min followed by 40 cycles at 95ºC/15 s, 60ºC/1 min in a reaction mixture that contained 1x Taqman Universal PCR Master Mix and 1x Assay Mix in a final volume of 20µl. The relative quantity of the gene targets was determined by the 2ΔΔCt method (Livak and Schmittgen, 2001) using Tbp as a housekeeping control.

Transcriptomic analysis. Total RNA was extracted (DNA-free) from FACS-sorted cells pooled from 8-10 animals per strain, by using miRNeasy Micro Kit (217084, Qiagen). RNAs were controlled using Nanodrop ND-1000 and Bioanalyzer 2100 Expert from Agilent, then 25 ng of RNA was used as input for labeled cRNA synthesis with the Low Input Quick Amp Labeling Kit (5190-2305, Agilent

Technologies) and the One-color microarray-based gene expression protocol, according to manufacturer´s instructions. Labeled cRNAs were hybridized to Agilent SurePrint G3 Mouse GE 8x60K Microarray Kit (G4852A, Agilent Technologies). The slides were scanned on a Tecan scanner MS200 and analyzed by Feature Extraction V.11.5.1.1.

Molecular signature enrichment analysis. The molecular signatures were taken from the gene set collection C5 of the version 3.0 of the Molecular Signatures Database (MSigDB) (Subramanian et al., 2005). The significance of the gene set of the different expressed genes was analyzed using an enrichment approach based on the hypergeometric distribution. The significance (p-value) of the gene set enrichment was calculated using the hypergeometric distribution. The multitest effect influence was corrected trough controlling the false discovery rate using the Benjamini-Hochberg correction at a significance level $\alpha=0.05$.

SUPPLEMENTAL FIGURES AND LEGENDS

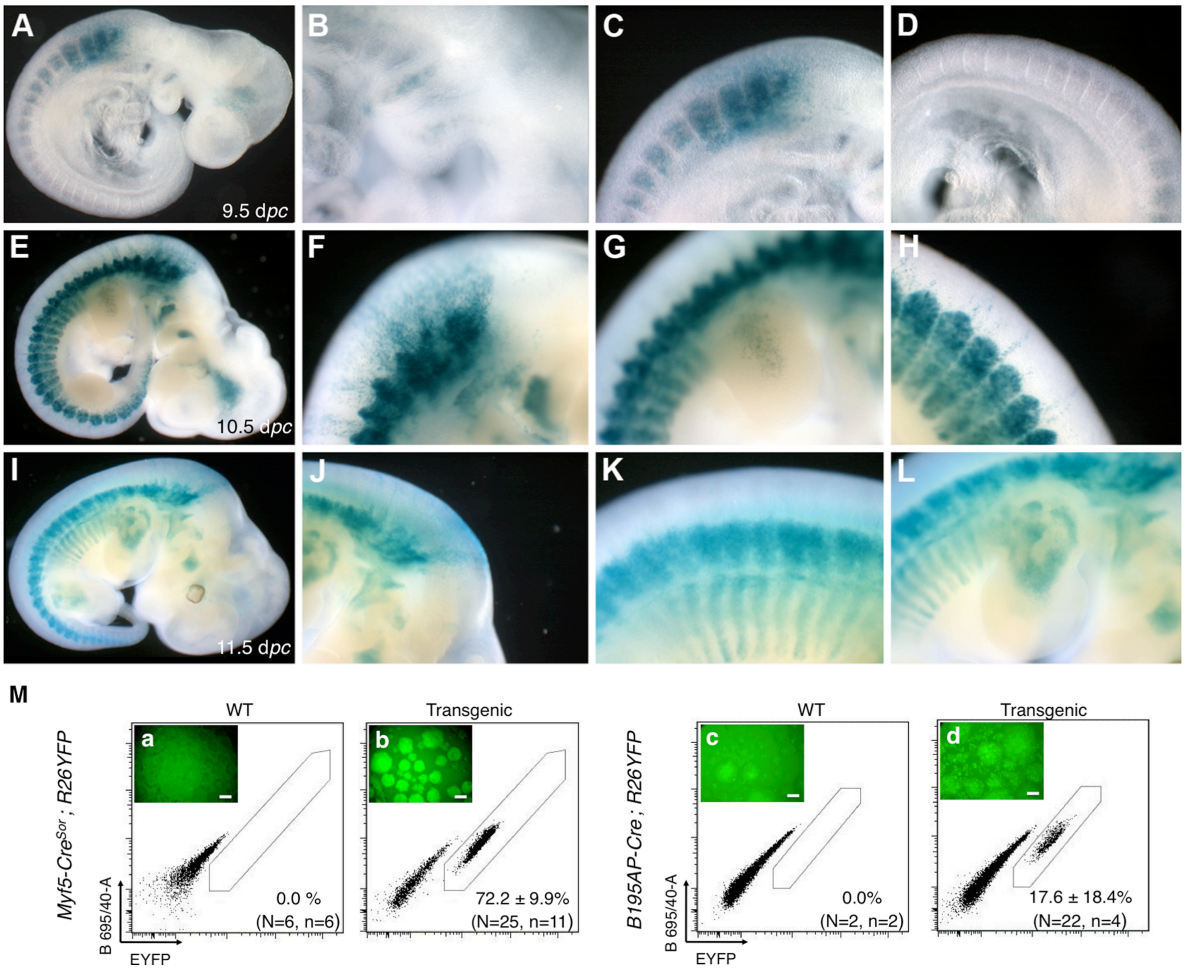

Figure S1. Time course of embryos carrying the *Myf5* reporter construct *B195AP-Cre* crossed with the *R26LACZ* strain, related to Figure 1. Representative mouse embryos (A, E, I) and close-ups from the same embryos (B-D, F-H, J-L) at 9.5d*pc* (A-D), 10.5d*pc* (E-H) and 11.5d*pc* (I-L). (A) β-Galactosidase staining can be detected at the known sites of *Myf5* expression at 9.5d*pc*, including the (B) mandibular and hyoid arches, (C) cervical somites and (D) the remaining somites with the exception of the 3 or 4 most recently formed; this apparent delay is likely caused by the time required to generate high levels of CRE protein in order to recombine the *R26LACZ* locus. (E) At 10.5d*pc* *Myf5+* cells can be detected in all muscle progenitor cells known to express *Myf5* at this stage, including all somites, branchial arches, hypoglossal chord and brain. (F) Interestingly, large numbers of *Myf5+* cells appear to migrate dorsally, into non-typical skeletal muscle locations. (G) *Myf5+* cells are also clearly visible in the forelimbs. (H) Migrating cells are not restricted to cervical positions but appear throughout the embryo but at positions always dorsal to the somites; note

that while migration in cervical positions does not follow any apparent pattern, migration at more caudal positions follows straight lines. (I) By 11.5dpc, most *Myf5+* cells are restricted to defined skeletal muscle locations such as the thoracic muscles, fore and hindlimb muscles, mandibular and hyoid arch derivatives. (J, K) Cells continue to migrate dorsal to the somites. (L) Detail of *Myf5+* cells in the forelimb. (M) Comparative analysis of EYFP+ cells by fluorescence and quantification by flow cytometry in dermal spheres isolated from *Myf5*^{SOR} and *B195AP* lineage tracing models. Left panels (a, c) show WT animal controls and right panels (b, d) transgenic animals. Insets, fluorescence images of dermal sphere cultures showing EYFP expression restricted to the transgenic animals. (Scale bars, 100 µm). Numbers represent mean±SD. The experiments were independently replicated as specified (N=mice; n=experiments).

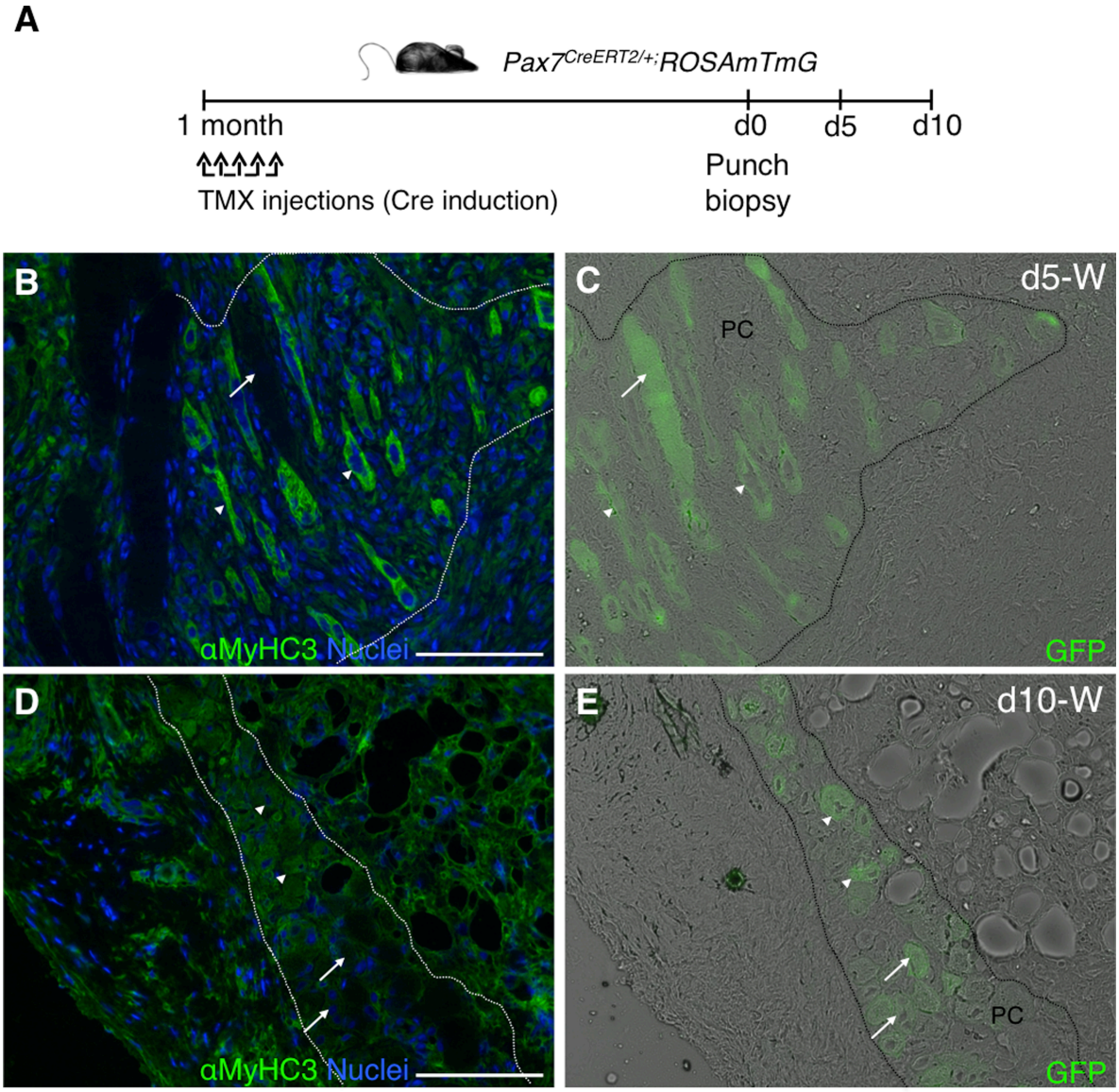

Figure S2. Presence of regenerative fibers in the *Panniculus carnosus* after wounding, related to Figure 3. (A) Outline of experimental design for the long-term induction of *Pax7* expression before punch biopsy is performed. (B-E) Histological sections of injured dorsal skin at day 5 (B-C) and at day 10 (D-E) post-wounding, were analyzed by immunofluorescence with anti-MyHC3 antibody showing regenerative fibers (B, D) and the GFP fluorescence showing *Pax7*-derived fibers (C,E). GFP+ MyHC3- cells are marked by arrows and GFP+ MyHC3+ cells are marked by arrowheads. Nuclei were counterstained with Hoechst 33258 (blue). Scale bars, 100 µm.

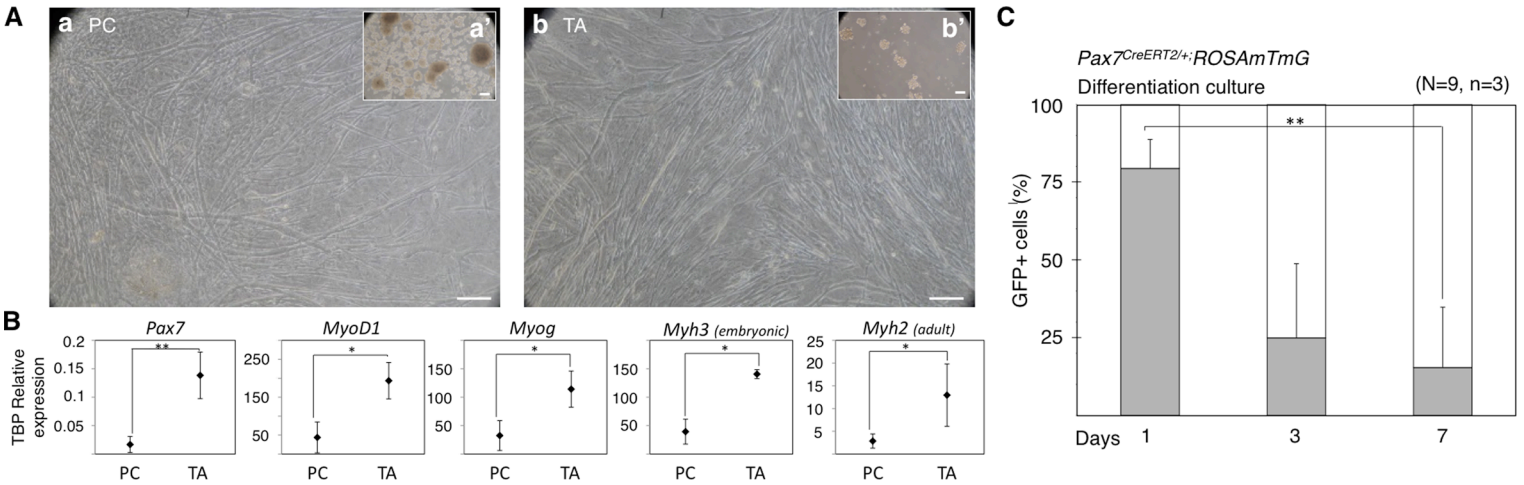

Figure S3. Comparison of limb muscle (TA)-derived and dermal muscle (PC)-derived myogenic differentiation cultures, related to Figure 5. (A) Morphologic aspects of sphere cultures of cells isolated from dermal PC muscle (a') and TA muscle (b'), and differentiated cultures of dermal PC (a) and TA muscle (b). (B) Quantitative real-time PCR (qRT-PCR) analysis for mRNA expression of myogenic markers *Pax7*, *MyoD1*, *Myogenin (Myog), MyH3 (embryonic MyHC),* and *MyH2 (adult MyHC)* in differentiated cultures from PC and TA. Expression is shown relative to *Tbp* and it is represented as the mean±SD of three independent mice. (C) Percentage of GFP+ mono- (grey bars) and multinucleated cells (white bars) at days 1, 3, and 7 of differentiation, as detected by immunofluorescence. Bars represent mean±SD. The experiments were independently replicated as specified (N=mice; n=experiments) (brackets: **=p<0.01; *=p<0.05).

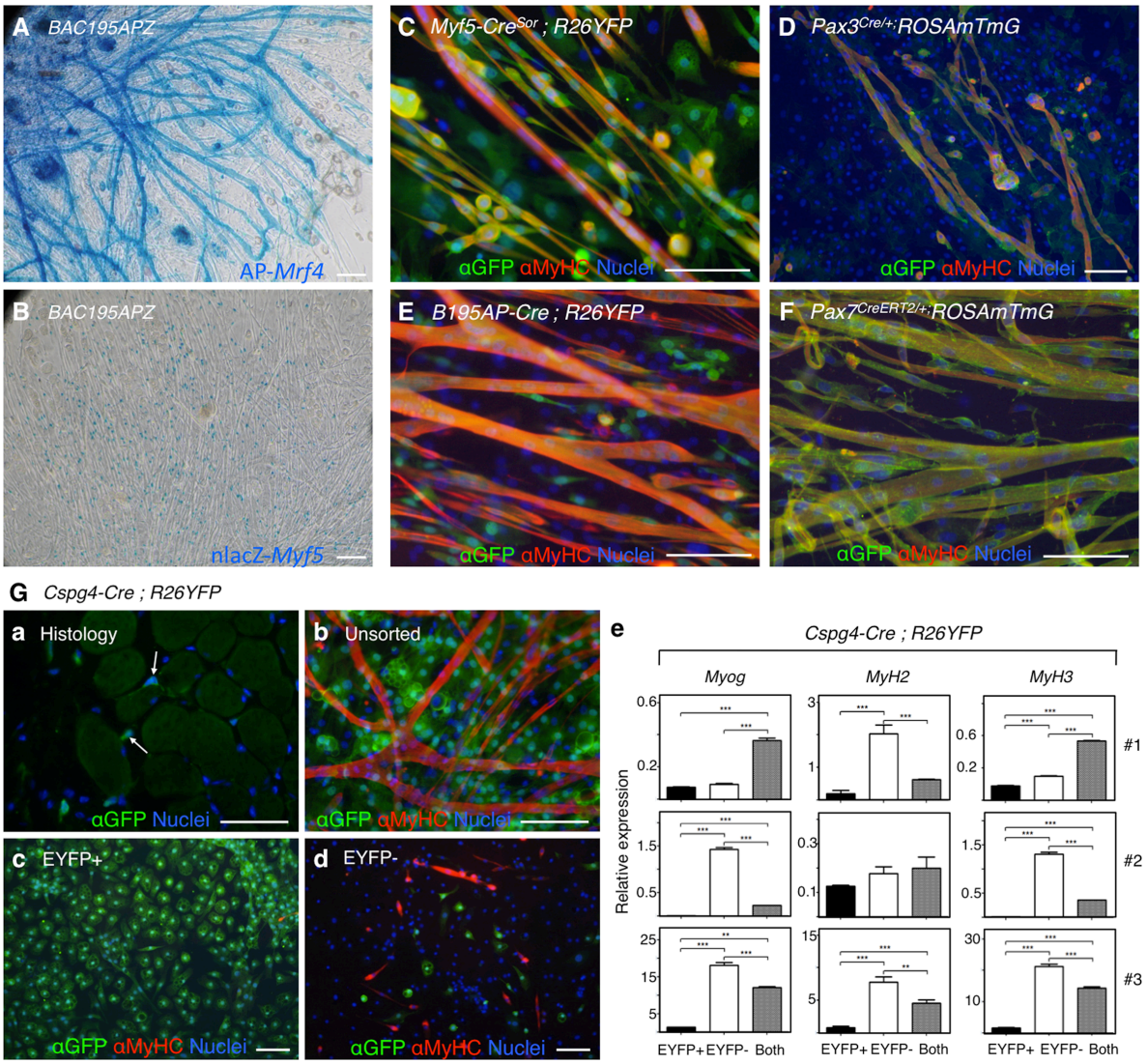

Figure S4. PC satellite cell progeny gives rise to dermis-derived myotubes, related to Figure 5. (A-B) Detection of AP-*Mrf4+* (panel A) and nlacZ-*Myf5+* (panel B) cells in differentiation cultures. (C-F) Contribution of Myf5^{SOR} (panel C), *Pax3Cre* (panel D), *B195AP-Cre* (panel E), and *Pax7^{CE}* (panel F)-derived cells to striated muscle was determined by immunofluorescence with anti-GFP (for EYFP expression), and sarcoplasmic anti-myosin heavy chain (MyHC, all fibers) antibodies. (G) Contribution of *Cspg4Cre*-derived cells to striated muscle. (a) *In situ* localization of *Cspg4*-derived cells in a histological section of dorsal skin by immunofluorescence with anti-GFP antibody. (b-d) Contribution of unsorted *Cspg4Cre*-derived cells (panel b) and FACS-sorted cell fractions [EYFP+ (panel c), EYFP- (panel d)] to striated muscle differentiation was measured by immunofluorescence with anti-GFP (for EYFP expression), and sarcoplasmic anti-myosin heavy chain (MyHC, all fibers) antibodies. Nuclei were counterstained with Hoechst 33258 (blue). (e)

Quantitative real-time PCR (qRT-PCR) analysis for mRNA expression of myogenic markers *Myogenin (Myog), MyH2 (adult MyHC)* and *MyH3 (embryonic MyHC)* from differentiated cultures of sorted cell fractions, "Both" fraction representing the mixture of EYFP+ and EYFP- sorted populations in the same percentages as in the original unsorted population. Expression is shown relative to the unsorted fraction (not shown). Bars represent mean±SD of a single experiment in which mRNA from eight mice was pooled (brackets: *p<0.05, **p<0.01, ***p<0.001). Scale bars in all immunofluorescence panels, 100 µm.

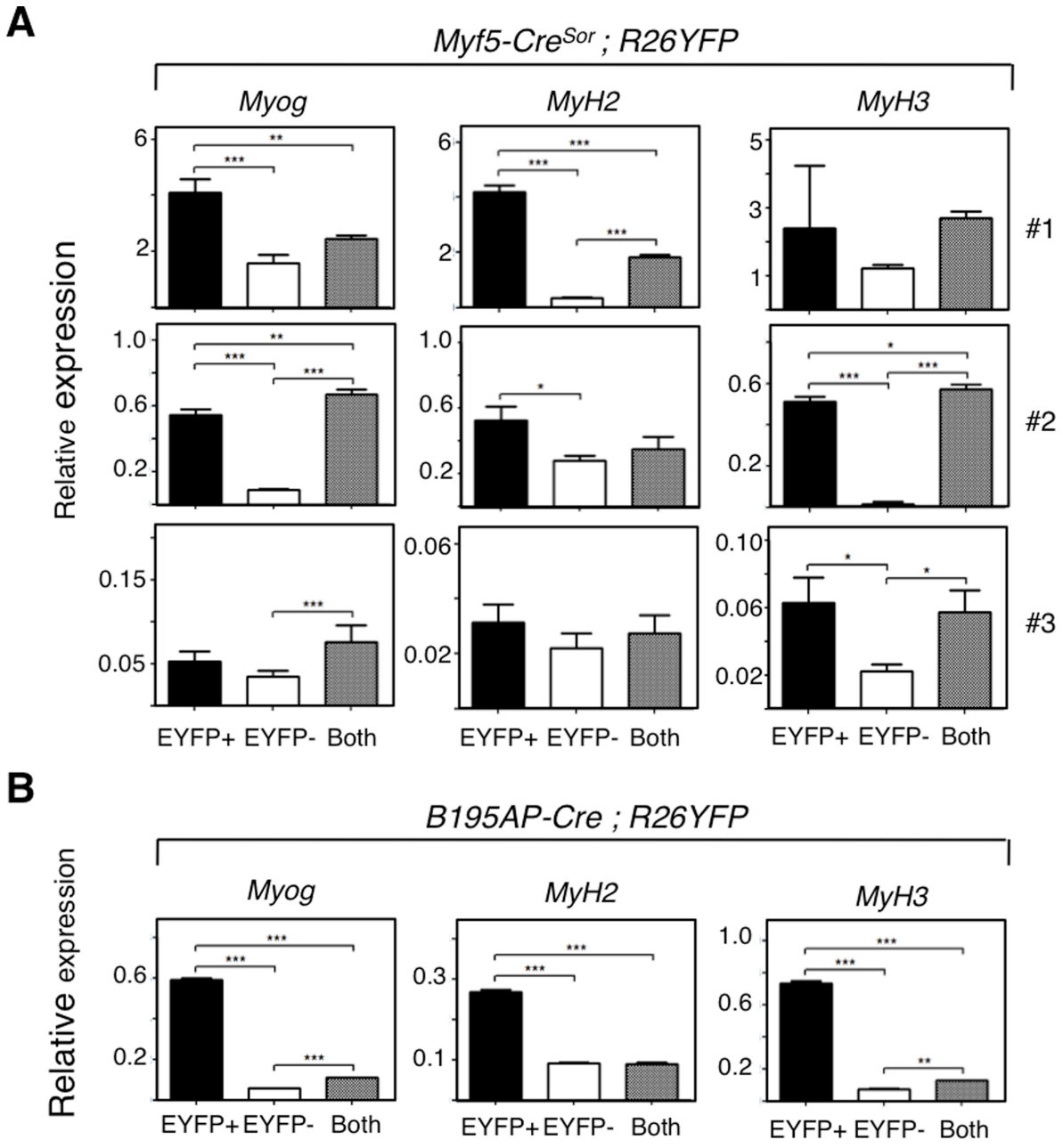

Figure S5. Quantitative contribution from *Myf5*^{SOR} and *B195AP*-traced cell lineages to striated muscle derivation, related to Figure 6. (A-B) Quantitative real-time PCR (qRT-PCR) analysis for mRNA expression of myogenic markers *Myogenin* (*Myog*), *MyH2 (adult MyHC)* and *MyH3 (embryonic MyHC)* from differentiated cultures of sorted cell fractions and "Both" fraction [representing the mixture of EYFP+ and EYFP- sorted populations in the same percentages as represented in the original cell population]. Expression is shown relative to the unsorted cell fraction (not shown). Chart bars represent mean±SD of three independent experiments (#1, #2, #3) in which mRNA from at least four mice was pooled (brackets: *p<0.05, **p<0.01, ***p<0.001).

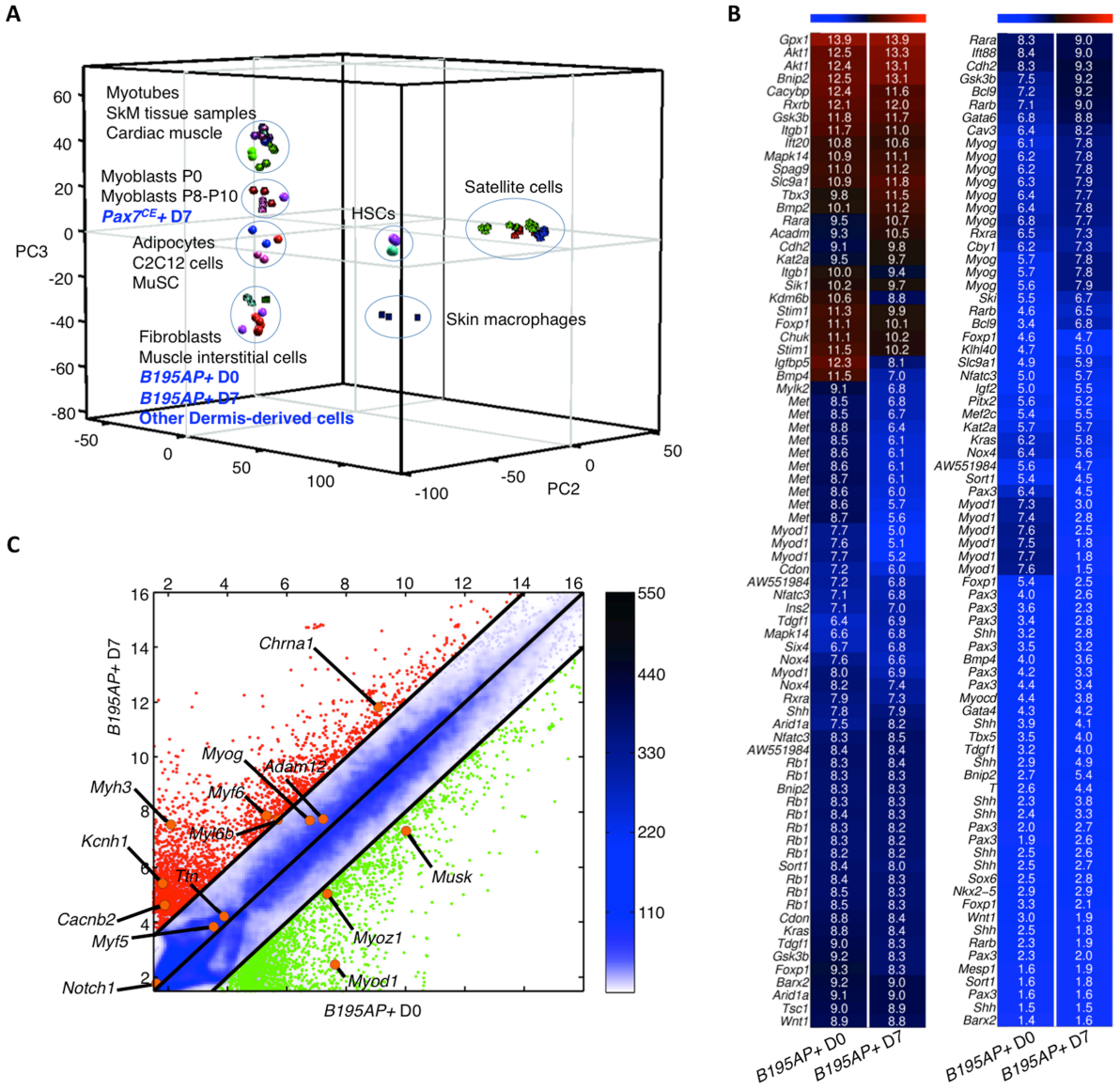

Figure S6. Transcriptomic analysis of *Myf5+* dermal myogenic precursors, related to Figure 6. Total RNAs from FACS-sorted dermal *B195AP*(+/-) and *Pax7*^{CE}(+/-) cell fractions were isolated at days 0 and 7 of proliferation culture. Total RNAs from dermal *Myf5*^{SOR}(+/-), *B195AP*(+/-) and *Cspg4*(+/-) cell fractions as well as from CD1 control mice were isolated. Since Syndecan-4 (Sdc4), a well-known satellite cell marker (Cornelison et al., 2001; Tanaka et al., 2009) was enriched in *Myf5*-EYFP+ cells (data not shown), *Myf5*^{SOR}(+/-), *B195AP*(+/-), *Cspg4*(+/-), and *CD1* control mice cells were fractionated using this marker as well. Microarray analyses were compared to database samples as detailed in Table S2. (A) Principal Component Analysis (PCA) of gene expression data. The 1st principal component (PC1) captures 47% of the gene expression variability. PC2 and PC3

capture 13 and 7.3% of the variability, respectively. (B) Heat maps showing the expression levels of the 154 probes (63 genes) associated with the GO category "striated muscle cell differentiation" in the *B195AP+* cells at day 0 (D0) and day 7 (D7). (C) Pairwise scatter plot of *B195AP+* cells at day 0 (D0) and day 7 (D7). The positions of some myogenic markers (*Myod1, Myoz1, Musk, Adam12, Myog, Ttn, Myf5, Notch1, Chrna1, Myl6b, Myf6, Myh3, Cacnb2,* and *Kcnh1*) are shown as orange dots. The color bar to the right indicates the scattering density. The gene expression levels are log2 scaled.

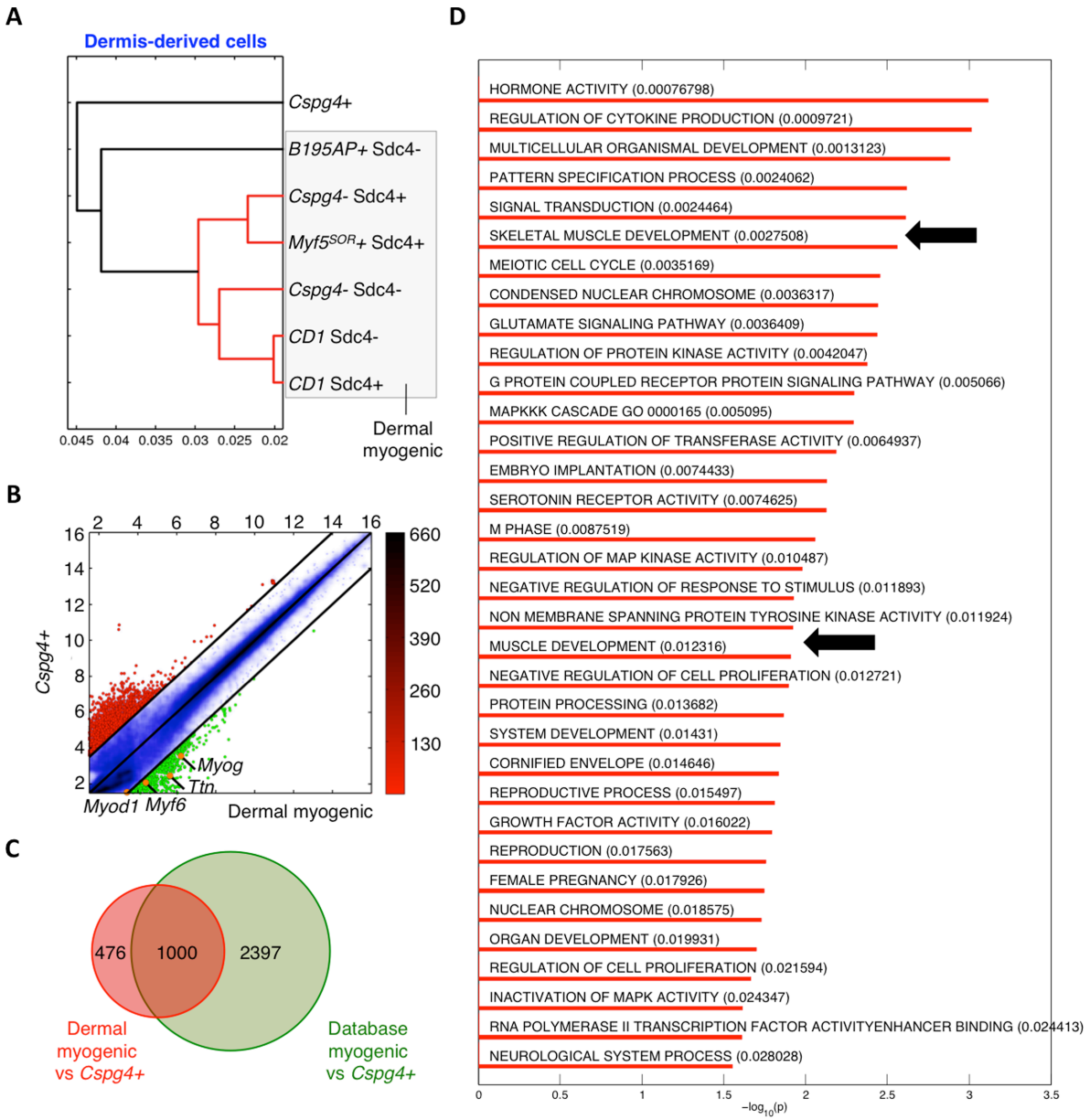

Figure S7. Transcriptomic analysis of dermal myogenic and non-myogenic precursor cell fractions, related to Figure 6. Total RNAs from dermal *Myf5*^{SOR}(+/-), *B195AP*(+/-) and *Cspg4*(+/-) cell fractions as well as from *CD1* control mice were isolated. Since Syndecan-4 (Sdc4), a well-known satellite cell marker (Cornelison et al., 2001; Tanaka et al., 2009) was enriched in *Myf5*-EYFP+ cells (data not shown), cells were fractionated using this marker as well. Microarray analyses were compared to database samples as detailed in Table S2. (A) Hierarchical clustering of samples performed using the correlation metric and the average linkage method. (B) Pairwise scatter plot. Genes upregulated in ordinates sample compared with abscissas samples are shown

in red circles; those downregulated are shown in green. The positions of some myogenic markers (*Myod1, Myf6, Ttn, Myog*) are shown as orange dots. The color bar to the right indicates the scattering density. The gene expression levels are log2 scaled. (C) Venn diagram showing overlap among (i) genes upregulated between dermal myogenic and *Cspg4+* cell fractions, and (ii) database myogenic and *Cspg4+* cell fractions. (D) Plot bar of the -log10(p) of the significant GSEA-enriched terms (p-values given in parentheses). Arrows point to muscle-related GSEA terms.

SUPPLEMENTAL TABLES

Supplemental Table S1. Mouse strains used in this study, related to Figures 1-7.

Abbreviated name	Full name	JAX stock number[1]	Charles River strain code[2]	Harlan order code[3]	Reference
B195AP^{Cre}	*BAC195AP-Cre*				This study
B195APZ	*BAC195APZ*				(Carvajal et al., 2001)
Bmi1$^{CreER/+}$	*B6;129-Bmi1$^{tm1(cre/ERT)Mrc}$/J*	010531			(Sangiorgi and Capecchi, 2008)
CD1	*Crl:CD1(ICR)*		022		
Cspg4^{Cre}	*B6;FVB-Tg(Cspg4-cre)1Akik/J*	008533			(Zhu et al., 2008)
Foxn1^{nu}	*Hsd:Athymic Nude-Foxn1^{nu}*			069(nu) 070(nu/+)	(Pantelouris, 1968)
Myf5^{CreSOR}	*B6.129S4-Myf5tm3(cre)Sor /J*	007893			(Tallquist et al., 2000)
Pax3$^{Cre/+}$	*B6;129-Pax3tm1(cre)Joe/J*	005549			(Engleka et al., 2005)
Pax3$^{GFP/+}$					(Relaix et al., 2005)
Pax3$^{IRESnLacZ/+}$					(Relaix et al., 2003)
Pax7$^{CreER2/+}$	*B6;129-Pax7tm2.1(cre/ERT2)Fan/J*	012476			(Lepper et al., 2009; Lepper and Fan, 2011; Lepper et al., 2011)
ROSAmTmG	*Gt(ROSA)26Sortm4(ACTB-tdTomato,-EGFP)Luo/J*	007676			(Muzumdar et al., 2007)
R26R	*FVB.129S4(B6)-Gt(ROSA)26Sor^{tm1Sor}/J*	009427			(Soriano, 1999)
R26R$^{GFP-DTA/+}$	*Gt(ROSA)26Sor$^{tm1(DTA)Jpmb}$/J*	006331			(Ivanova et al., 2005)
R26YFP	*B6.129X1-Gt(ROSA)26Sortm1(EYFP)Cos/J*	006148			(Srinivas et al., 2001)

[1] http://jaxmice.jax.org
[2] http://www.criver.com
[3] http://www.harlan.com

Supplemental Table S2. Arrays used for transcriptomic analyses, related to Figures S6 and S7.

GSM #	Description	Reference
GSM990708	Cardiomyocytes - 129SvEv/C57BL/6 wild type mice cardiomyocytes 16hr after PBS injection.	(Zhang et al., 2012)
GSM990709		
GSM990710		
GSM997165	Myoblastic - C2C12 myoblastic cell line.	(Davidovic et al., 2013)
GSM997166		
GSM1541931	Myoblasts P0 - C57BL/6J mice primary myoblasts in proliferation conditions at passage 0.	Carrió and Suelves, unpublished
GSM1541932		
GSM1541933		
GSM1541934	Myoblasts Prolif - C57BL/6J mice primary myoblasts in proliferation conditions at passage 8-10.	
GSM1541935		
GSM1541936		
GSM1541937	Myotubes D1 - C57BL/6J mice primary myotubes differentiation conditions at day 1.	
GSM1541938		
GSM1541939		
GSM1541940	Myotubes D2 - C57BL/6J mice primary myotubes differentiation conditions at day 2.	
GSM1541941		
GSM1541942		
GSM1541943	Myotubes D4 - C57BL/6J mice primary myotubes differentiation conditions at day 4.	
GSM1541944		
GSM1541945		
GSM1541949	Skeletal Muscle - NOD/ShiLtj mice skeletal muscle.	
GSM1541946	Quadriceps - 129Sv/C57BL/6J mice quadriceps muscle.	
GSM1541947		
GSM1541948		
GSM856087	MuSC - C57BL/6J DMD/MDX mice FACS sorted cells, CD34+/a7-integrin+/Sca1-.	Roy M Williams, unpublished
GSM856083	Muscle Interstitial - C57BL/6J DMD/MDX mice FACS sorted cells, CD34+/a7-integrin+/Sca1+.	
GSM856084		
GSM1253022	Skeletal Muscle AR97Q - C57BL/6J AR-97Q mice skeletal muscle.	(Iida et al., 2015)
GSM1253023		
GSM1253024		
GSM1299431	Satellite Young 1 - C57BL/6 2 month aged mice FACS sorted satellite cells.	(Sousa-Victor et al., 2014)
GSM1299432		
GSM1299433		
GSM1299438	Satellite Young 2 - C57BL/6 2 month aged mice FACS sorted satellite cells.	
GSM1299439		
GSM1299440		
GSM1299452	Satellite Young 3 - C57BL/6 2 month aged mice FACS sorted satellite cells.	
GSM1299453		
GSM1299454		
GSM1299458	Satellite WTBmi1 4 - FVB wild type 2 month aged mice FACS sorted satellite cells.	

GSM1299459		
GSM1299460		
GSM1299441	Satellite Old 2 - C57BL/6 23 month aged mice FACS sorted satellite cells.	
GSM1299442		
GSM1299443		
GSM1299455	Satellite Adu 3 - C57BL/6 6 month aged mice FACS sorted satellite cells.	
GSM1299456		
GSM1299457		
GSM1299434	Satellite Ger 1 - C57BL/6 28 month aged mice FACS sorted satellite cells.	
GSM1299435		
GSM1299436		
GSM1299444	Satellite Ger 2 - C57BL/6 28 month aged mice FACS sorted satellite cells.	
GSM1299445		
GSM1220789	Fibroblast - C57/Bl6-J mice tail fibroblasts cells.	(Furtado et al., 2014)
GSM1220790		
GSM1220791		
GSM1037932	Adipocytes - 3T3-L1 cultured mature adipocytes treated with physiological saline	(Chew et al., 2014)
GSM1037933		
GSM1109740	HSC-CD41- - Freshly FACS sorted HSCs from mouse bone marrow, Lin-sca1+ckit+flt3-CD41-	(Gekas and Graf, 2013)
GSM1109741		
GSM1109742		
GSM1109743	HSC-CD41+ - Freshly FACS sorted HSCs from mouse bone marrow, Lin-sca1+ckit+flt3-CD41+	
GSM1109744		
GSM1109745		
GSM1400758	Macrophages - CD1 skin resident macrophages	Castellana and Perez-Moreno, unpublished
GSM1400759		
GSM1400760		

SUPPLEMENTAL REFERENCES

Carvajal, J.J., Cox, D., Summerbell, D., and Rigby, P.W.J. (2001). A BAC transgenic analysis of the Mrf4 / Myf5 locus reveals interdigitated elements that control activation and maintenance of gene expression during muscle development. Development *1868*, 1857-1868.

Carvajal, J.J., Keith, A., and Rigby, P.W. (2008). Global transcriptional regulation of the locus encoding the skeletal muscle determination genes Mrf4 and Myf5. Genes & development *22*, 265-276.

Chew, S.H., Okazaki, Y., Nagai, H., Misawa, N., Akatsuka, S., Yamashita, K., Jiang, L., Yamashita, Y., Noguchi, M., Hosoda, K.*, et al.* (2014). Cancer-promoting role of adipocytes in asbestos-induced mesothelial carcinogenesis through dysregulated adipocytokine production. Carcinogenesis *35*, 164-172.

Cornelison, D.D., Filla, M.S., Stanley, H.M., Rapraeger, A.C., and Olwin, B.B. (2001). Syndecan-3 and syndecan-4 specifically mark skeletal muscle satellite cells and are implicated in satellite cell maintenance and muscle regeneration. Dev Biol *239*, 79-94.

Dahlqvist, C., Blokzijl, A., Chapman, G., Falk, A., Dannaeus, K., Ibanez, C.F., and Lendahl, U. (2003). Functional Notch signaling is required for BMP4-induced inhibition of myogenic differentiation. Development *130*, 6089-6099.

Davidovic, L., Durand, N., Khalfallah, O., Tabet, R., Barbry, P., Mari, B., Sacconi, S., Moine, H., and Bardoni, B. (2013). A novel role for the RNA-binding protein FXR1P in myoblasts cell-cycle progression by modulating p21/Cdkn1a/Cip1/Waf1 mRNA stability. PLoS genetics *9*, e1003367.

DeChiara, T.M., Bowen, D.C., Valenzuela, D.M., Simmons, M.V., Poueymirou, W.T., Thomas, S., Kinetz, E., Compton, D.L., Rojas, E., Park, J.S.*, et al.* (1996). The receptor tyrosine kinase MuSK is required for neuromuscular junction formation in vivo. Cell *85*, 501-512.

Engleka, K.A., Gitler, A.D., Zhang, M., Zhou, D.D., High, F.A., and Epstein, J.A. (2005). Insertion of Cre into the Pax3 locus creates a new allele of Splotch and identifies unexpected Pax3 derivatives. Dev Biol *280*, 396-406.

Furtado, M.B., Costa, M.W., Pranoto, E.A., Salimova, E., Pinto, A.R., Lam, N.T., Park, A., Snider, P., Chandran, A., Harvey, R.P.*, et al.* (2014). Cardiogenic genes expressed in cardiac fibroblasts contribute to heart development and repair. Circulation research *114*, 1422-1434.

Gekas, C., and Graf, T. (2013). CD41 expression marks myeloid-biased adult hematopoietic stem cells and increases with age. Blood *121*, 4463-4472.

Halevy, O., and Lerman, O. (1993). Retinoic acid induces adult muscle cell differentiation mediated by the retinoic acid receptor-alpha. Journal of cellular physiology *154*, 566-572.

Iida, M., Katsuno, M., Nakatsuji, H., Adachi, H., Kondo, N., Miyazaki, Y., Tohnai, G., Ikenaka, K., Watanabe, H., Yamamoto, M.*, et al.* (2015). Pioglitazone suppresses neuronal and muscular degeneration caused by polyglutamine-expanded androgen receptors. Human molecular genetics *24*, 314-329.

Ivanova, A., Signore, M., Caro, N., Greene, N.D., Copp, A.J., and Martinez-Barbera, J.P. (2005). In vivo genetic ablation by Cre-mediated expression of diphtheria toxin fragment A. Genesis *43*, 129-135.

Lepper, C., Conway, S., and Fan, C. (2009). Adult satellite cells and embryonic muscle progenitors have distinct genetic requirements. Nature *460*, 627-631.

Lepper, C., and Fan, C.-m. (2011). Inducible lineage tracing of Pax7-descendant cells reveals embryonic origin of adult satellite cells. Genesis *48*, 424-436.

Lepper, C., Partridge, T.a., and Fan, C.-M. (2011). An absolute requirement for Pax7-positive satellite cells in acute injury-induced skeletal muscle regeneration. Development *138*, 3639-3646.

Lovett, F.A., Gonzalez, I., Salih, D.A., Cobb, L.J., Tripathi, G., Cosgrove, R.A., Murrell, A., Kilshaw, P.J., and Pell, J.M. (2006). Convergence of Igf2 expression and adhesion signalling via RhoA and p38 MAPK enhances myogenic differentiation. J Cell Sci *119*, 4828-4840.

Muzumdar, M., Tasic, B., Miyamichi, K., Li, L., and Luo, L. (2007). A global double-fluorescent Cre reporter mouse. Genesis *605*, 593-605.

Ono, Y., Calhabeu, F., Morgan, J.E., Katagiri, T., Amthor, H., and Zammit, P.S. (2011). BMP signalling permits population expansion by preventing premature myogenic differentiation in muscle satellite cells. Cell death and differentiation *18*, 222-234.

Pantelouris, E.M. (1968). Absence of thymus in a mouse mutant. Nature *217*, 370-371.

Relaix, F., Polimeni, M., Rocancourt, D., Ponzetto, C., Schafer, B.W., and Buckingham, M. (2003). The transcriptional activator PAX3-FKHR rescues the defects of Pax3 mutant mice but induces a myogenic gain-of-function phenotype with ligand-independent activation of Met signaling in vivo. Genes & development *17*, 2950-2965.

Relaix, F., Rocancourt, D., Mansouri, A., and Buckingham, M. (2005). A Pax3/Pax7-dependent population of skeletal muscle progenitor cells. Nature *435*, 948-953.

Rozwadowska, N., Kolanowski, T., Wiland, E., Siatkowski, M., Pawlak, P., Malcher, A., Mietkiewski, T., Olszewska, M., and Kurpisz, M. (2013). Characterisation of nuclear architectural alterations during in vitro differentiation of human stem cells of myogenic origin. PLoS One *8*, e73231.

Sambasivan, R., Comai, G., Le Roux, I., Gomes, D., Konge, J., Dumas, G., Cimper, C., and Tajbakhsh, S. (2013). Embryonic founders of adult muscle stem cells are primed by the determination gene Mrf4. Dev Biol *381*, 241-255.

Sangiorgi, E., and Capecchi, M.R. (2008). Bmi1 is expressed in vivo in intestinal stem cells. Nature genetics *40*, 915-920.

Sharples, A.P., Al-Shanti, N., Lewis, M.P., and Stewart, C.E. (2011). Reduction of myoblast differentiation following multiple population doublings in mouse C2 C12 cells: a model to investigate ageing? Journal of cellular biochemistry *112*, 3773-3785.

Sousa-Victor, P., Gutarra, S., Garcia-Prat, L., Rodriguez-Ubreva, J., Ortet, L., Ruiz-Bonilla, V., Jardi, M., Ballestar, E., Gonzalez, S., Serrano, A.L*., et al.* (2014). Geriatric muscle stem cells switch reversible quiescence into senescence. Nature *506*, 316-321.

Srinivas, S., Watanabe, T., Lin, C.S., William, C.M., Tanabe, Y., Jessell, T.M., and Costantini, F. (2001). Cre reporter strains produced by targeted insertion of EYFP and ECFP into the ROSA26 locus. BMC developmental biology *1*, 4.

Stern-Straeter, J., Bonaterra, G.A., Hormann, K., Kinscherf, R., and Goessler, U.R. (2009). Identification of valid reference genes during the differentiation of human myoblasts. BMC molecular biology *10*, 66.

Subramanian, A., Tamayo, P., Mootha, V.K., Mukherjee, S., Ebert, B.L., Gillette, M.A., Paulovich, A., Pomeroy, S.L., Golub, T.R., Lander, E.S*., et al.* (2005). Gene set enrichment analysis: a knowledge-based approach for interpreting genome-wide expression profiles. Proceedings of the National Academy of Sciences of the United States of America *102*, 15545-15550.

Swaminathan, S., Ellis, H.M., Waters, L.S., Yu, D., Lee, E.C., Court, D.L., and Sharan, S.K. (2001). Rapid engineering of bacterial artificial chromosomes using oligonucleotides. Genesis *29*, 14-21.

Tallquist, M.D., Weismann, K.E., Hellstrom, M., and Soriano, P. (2000). Early myotome specification regulates PDGFA expression and axial skeleton development. Development *127*, 5059-5070.

Tanaka, K.K., Hall, J.K., Troy, A.A., Cornelison, D.D., Majka, S.M., and Olwin, B.B. (2009). Syndecan-4-expressing muscle progenitor cells in the SP engraft as satellite cells during muscle regeneration. Cell Stem Cell *4*, 217-225.

Voronova, A., Coyne, E., Al Madhoun, A., Fair, J.V., Bosiljcic, N., St-Louis, C., Li, G., Thurig, S., Wallace, V.A., Wiper-Bergeron, N*., et al.* (2013). Hedgehog signaling regulates MyoD expression and activity. The Journal of biological chemistry *288*, 4389-4404.

Zhang, S., Liu, X., Bawa-Khalfe, T., Lu, L.S., Lyu, Y.L., Liu, L.F., and Yeh, E.T. (2012). Identification of the molecular basis of doxorubicin-induced cardiotoxicity. Nat Med *18*, 1639-1642.

Zhu, X., Hill, R.A., and Nishiyama, A. (2008). NG2 cells generate oligodendrocytes and gray matter astrocytes in the spinal cord. Neuron glia biology *4*, 19-26.